Spring 5-15-2020

Blood Flow Simulation of Particle Trapping in Models of Arterial Bifurcations

Qihang Xu

WASHINGTON UNIVERSITY IN ST. LOUIS
James McKelvey School of Engineering
Department of Mechanical Engineering and Materials Science

Thesis Examination Committee:

Dr. Ramesh K. Agarwal, Chair

Dr. David Peters

Dr. Swami Karunamoorthy

Blood Flow Simulations of Particle Trapping in Models of Arterial Bifurcations

by

Qihang Xu

A thesis presented to the James McKelvey School of Engineering
of Washington University in St. Louis in partial fulfillment of the
requirements for the degree of
Master of Science

May 2020

Saint Louis, Missouri

Table of Contents

List of Figures iv

List of Tables vi

Nomenclature vii

Acknowledgments viii

Dedication ix

Abstract x

1 Introduction 1
- 1.1 Overview 1
- 1.2 Outline 2
- 1.3 Scope of the Thesis 3

2 Laminar & Tubulent Flow 4
- 2.1 Overview 4
- 2.2 Governing Equations 4
- 2.3 Turbulence Modeling 5
  - 2.3.1 Reynolds-Averaged Navier-Stokes (RANS) Equations 5
  - 2.3.2 SST k- ω Turbulence Model 6
  - 2.3.3 Wray- Agarwal Turbulence Model 6

3 Mechanism of Particle Trapping 7
- 3.1 Physics of Particle Trapping 7
- 3.2 Theoretical Model of Force Balance 8
- 3.3 Particle Trapping Probability 9

4 Particle Trapping in T-Junction 10
- 4.1 Mechanism of Particle Trapping in T-Junction at low Reynolds Numbers 10
  - 4.1.1 Overview 10
  - 4.1.2 Influence of Particle Diameter in Particle Trapping 14
  - 4.1.3 Influence of Reynolds Number in Particle Trapping 16
- 4.2 Mechanism of Particle Trapping in T-Junction at High Reynolds Number 19
- 4.3 Validation 23

5 Particle Trapping in Y-Junction 27
- 5.1 Mechanism of Particle Trapping in Y-Junction at low Reynolds Numbers 27
  - 5.1.1 Overview 27
  - 5.1.2 Y-Junction Flow with Stenosis 30

5.1.3 Influence of Bifurcation Angle (BA) on Particle Trapping....33
5.2 Validation....36

6 Conclusions....39

7 Future Work....40

References....41

Vita....43

List of Figures

Figure 1.1 Particle Trapping Phenomenon in T-Junction 1
Figure 4.1 Geometry of T-Junction with Circular Cross-section & Structured Grids inside T-Junction 11
Figure 4.2 Refined Boundary Layer at Inlet Pipe & Outlet Pipe 11
Figure 4.3 Parabolic Velocity Profile at Inlet 12
Figure 4.4 Pressure Contours, Velocity Contours, Wall Shear Stress Contours & Streamlines in T-Junction Flow (Re = 360) 13
Figure 4.5 Axial Pressure Gradient along Vortex Core Line 14
Figure 4.6 Particle Tracking of Different Particle Diameters in T-Junction (Re = 360) 15
Figure 4.7 Particle Trapping at Different Reynolds Numbers in T-Junction at Re =150, 250, 360 & 480 18
Figure 4.8 Pressure Contours, Velocity Contours, Wall Shear Stress Contours & Streamlines for Turbulent Flow 21
Figure 4.9 Pressure Gradient and Axial Velocity in the Vortex Core Line in Turbulent T-Junction Flow 22
Figure 4.10 Particle Trapping for Re = 3000 Using SST k-ω Model & WA Model 23
Figure 4.11: Physical Model for CFD Validation Case (T-Junction) 23
Figure 4.12 Mesh & Refined Boundary Layer Region of the T-Junction 24
Figure 4.13 Streamlines and Vortex Structure for Re = 150 25
Figure 4.14 Axial Pressure Gradient Versus X Position for Re = 150, 200 and 250 25
Figure 4.15 Variation in Axial Pressure Gradient with X along the Vortex Core Line [1] 26
Figure 5.1 Geometry & Mesh of Y-Junction 27
Figure 5.2 Pressure Contours, Velocity Contours, Wall Shear Stress Contours and Streamlines in Y-Junction Laminar Flow 29
Figure 5.3 Particle Trapping in Y- Junction Flow at Re = 360, 420, 480 & 540 30
Figure 5.4 Geometry & Mesh in the Bifurcation Model with Stenosis 31
Figure 5.5 Velocity Distributions at Various Pipe Cross – Sections in Y-Junction Flow with and without Stenosis 32
Figure 5.6 Vorticity Distributions at Various Pipe Cross-Sections in Y-Junction Flow with and without Stenosis 33

Figure 5.7 Particle Trapping in Different Models at BA= 100°, 95°, 92.5°, 87.5°, 85° and 80° 35
Figure 5.8 Geometry of Y-Junction for CFD Validation 36
Figure 5.9 Pressure Contours, Velocity Contours, Wall Shear Stress Contours and Streamlines for Lu's Y-Junction Model 37
Figure 5.10 WSS Distribution at Line A and Simulation Results from Omid Arjmandi -Tash et al. [8] 38

List of Tables

Table 5.1 Percentage of Particles Trapped in Models with Different Bifurcation Angles.....35

Nomenclature

CFD	Computational Fluid Dynamics
PDE	Partial Differential Equation
U	Velocity Vector
D	Lateral Size or Diameter of Inlet
L	Length of The Pipes
Re	Reynolds Number
p	Static Pressure
dP/dX	Axial Pressure Gradient
ρ	Density of Fluid or Particles
μ	Viscosity of Fluid
Q	Mass Flow Rate at Inlet
WSS	Wall Shear Stress
BA	Bifurcation Angle

Acknowledgments

First, I am very grateful to Dr. Ramesh Agarwal for his professional guidance, effective suggestions and continuous encouragement.

I am also grateful to Dr. Peters and Dr. Karunamoorthy for serving on my thesis committee.

I am also grateful to my parents for their care and love for last 24 years.

Finally, I would like to thank my friends in CFD lab for their enthusiastic help and advice.

Qihang Xu

Washington University in St. Louis
May 2020

Dedicated to my family

ABSTRACT

Blood Flow Simulation of Particle Trapping in Models of Arterial Bifurcations

Qihang Xu
Master of Science in Mechanical Engineering
Washington University in St. Louis, 2020
Research Advisor: Professor Ramesh K. Agarwal

This thesis describes the particle trapping mechanism in blood flow in different arterial bifurcation models. For validation of CFD calculations, a T-junction model and a Y-junction model are analyzed. In both the models, there is one inlet pipe with two outlet pipes creating a symmetric bifurcation at some angle from the centerline of the inlet pipe. Naiver-Stokes (RANS) equations are solved for single phase laminar flow using the commercial CFD software ANSYS Fluent. After validation, Eulerian simulations are performed by using the Discrete Phase Model (DPM) for two-phase flow with particles injected in different bifurcation models with bifurcation angle of an outlet pipe varying from 80° to 100° w.r.t the centerline of the inlet pipe (90° being the bifurcation angle of T-junction). By changing the average Reynolds number of the flow and the injected particle diameters, the mechanism of particle trapping is investigated in laminar flow. The contours of velocity magnitude, pressure and wall shear stress are also obtained and analyzed. It is found that the particle trapping increases as the bifurcation angle decreases from 90° and becomes negligible as the bifurcation angle increases from 90°. This is a very important result which has never been reported in the previous literature. In addition, turbulent flow computations for T-junction flow are performed using the SST k-ω and Wray-Agarwal turbulence models. Finally, the influence of stenosis in Y-Junction is studied and analyzed. The results have implications in understanding the hemodynamic flows in arterial bifurcations without and with stenosis.

Chapter 1 Introduction

1.1 Overview

Bifurcations occur in many pipe systems which split the flow into different branches, e.g. blood flow in vascular systems [1-2]. In past several years, particle trapping in bifurcation flows has been a topic of significant interest in the study of blood transport. In hemodynamics, low-density particles and bubbles such as gas [3-4] are very easily trapped in the bifurcations of the vessels and finally form gas embolisms. According to Vigolo et al. [1], when mean inlet flow Reynolds number is above 200, low-density particles will be trapped near the T-junction and will be transported slowly in the outlet pipes over a relatively long time. This phenomenon is attributed to the density difference between the particles and the fluid and distribution of velocity and pressure fields inside the T-junction.

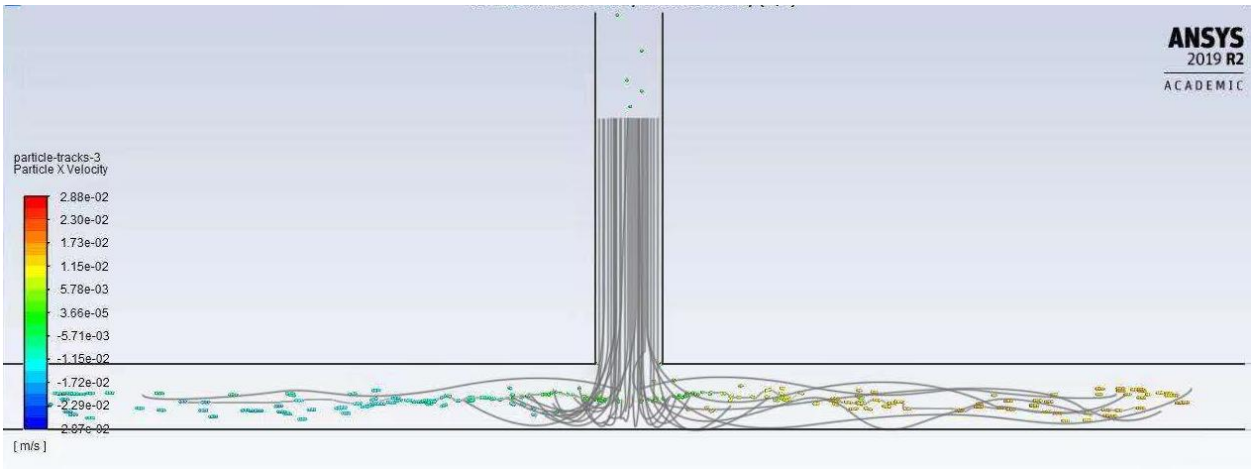

Figure 1.1 Particle Trapping Phenomenon in T-Junction Flow

Based on single phase fluid simulation in T-junction, when Re > 50, two counter-rotating vortices begin to form near the T-junction and are distributed symmetrically in the pipe. When Re > 250, the pressure increases in the vortex structure which leads to an adverse axial pressure gradient. As axial velocity at the vortex core decreases, low-density particles get trapped there. The vortex core is determined as the position which has a local minimum pressure in y-z cross-section along the x axis of the outlet pipe. When Re > 360, the fluid velocity reverses at a certain position which signifies the vortex breakdown [5-7]. Vigolo et al. [1] also conducted an experiment to study the mechanism of particle trapping using a 90° bifurcation with a square cross-section duct with lateral size ranging from

0.4 to 4.8 mm. It was found that at low inlet Reynolds number, no particle trapping occurred until the Reynolds number was increased to 200. When 200 < Re < 550, permanent particle trapping could occur. But only the big particles can get into the vortex core and are trapped for a long time while small particles rotate keeping away from the vortex core line. When 550 < Re < 900, particles are trapped but the flow becomes unsteady.

There are also some studies with focus on Y-junction flows. Arjmandi-Tash et al. [8] performed simulations to study the impact of different bifurcation angles. They found that the change in angle has great influence on Wall Shear Stress (WSS) distribution. CFD results in this thesis are compared with their computations for the purpose of validation and show good agreement. Antonova [9] also studied the effect of stenosis in Y-junction flows and concluded that the vorticity patterns are more likely to be influenced than the velocity magnitudes due to the presence of stenosis. The detailed simulations presented in this thesis match her conclusions quite well.

1.2 Outline

This thesis investigates the general mechanism of particle trapping in different bifurcation models by numerical simulation. The results for T-junction flow generally match the results of Vigolo et al. [1]. When Re = 360, particle trapping occurs only for particles with diameters above 5% of pipe's diameter. The probability of a particle getting trapped increases as the particle gets bigger. But when particle diameter is fixed at 5% of pipe's diameter, particle trapping occurs only in the flow with Reynolds number above 250. A higher probability of particle trapping occurs in laminar flows with higher Reynolds number. Computations are also performed for bifurcation angle of an outlet pipe varying from 80^o to 100^o w.r.t the centerline of the inlet pipe (90^o being the bifurcation angle of T-junction). It is found that the particle trapping increases as the bifurcation angle decreases from 90^o and becomes negligible as the bifurcation angle increases from 90^o. In addition, computations are also performed for turbulent flow at Re = 3000; SST k-ω [10] and Wray-Agarwal turbulence models [11] are used to solve the RANS equations. The turbulent flow computations show a totally different flow field and more importantly particle trapping does not occur in both T- and Y-junction flows. Finally, the effect of stenosis in Y-junction flow is studied and the results generally match those of Antonova [9].

The contents of various chapters are described below.

Chapter 2: Laminar & Turbulent Flow: This chapter briefly introduces basic concepts of laminar and turbulent flows. The governing PDEs of fluid dynamics including Reynolds-Averaged Navier-Stokes (RANS) equations and some turbulence models are briefly described.

Chapter 3: Mechanism of Particle Trapping: This chapter reviews the relevant studies and provides detailed description of the physics of particle trapping. It describes how force balance is achieved on particles trapped inside the vortex core. Force balance equations include axial force balance equation and radial force balance equation. The factors influencing the particle trapping include particle diameter, fluid Reynolds number and the bifurcation angle.

Chapter 4: Mechanisms of Particle Trapping in T-Junction Flow: This chapter describes how particle trapping can be influenced by Reynolds number and particle diameters in T-junction flow. The computations are validated against experimental data. The contours of pressure, velocity and WSS are provided. It is shown that both SST k-ω and WA turbulence models give similar results.

Chapter 5: Mechanism of Particle Trapping in Y-Junction Flow: Detailed calculations show that at low Reynolds numbers, particle trapping only occurs when bifurcation angle is less than 90^{o}. Computations are also performed for a Y-junction with stenosis; the simulations match predictions of other investigators quite well showing that the stenosis has a larger influence on vorticity than velocity field.

Chapter 6 & Chapter 7: Conclusions &Future work: Chapter 6 provides conclusions based on research conducted in the thesis and Chapter 7 provides a description of the research issues that should be addressed in the future work.

1.3 Scope of the Thesis

All bifurcation models considered in this thesis are built and modified using the software SOLIDWORKS and are meshed by ICEM-CFD. Numerical simulations are conducted by using the commercial CFD software ANSYS Fluent and post processing is done in ANSYS CFD Post. Both laminar and turbulent flow cases are considered and compared with experimental data and computations of other investigators where available. Turbulent flow computations are performed using the SST k-ω and Wray-Agarwal turbulence models. After recording the numerical data from Fluent, it is imported into Microsoft Excel for further processing into quantities of interest.

Chapter 2 Laminar & Turbulent Flows

2.1 Overview

Laminar flow occurs when fluid flows at relatively low velocity in pipes. Adjacent layers slide parallel to each other without fluctuations and never mix with each other. Since the fluid particles move in an orderly fashion and always parallel to the walls, no cross-currents, or eddies or swirls occur in laminar flows. Thus, the shear stress in laminar flow is mainly governed by the Stokes hypothesis that is the shear stress is linearly proportional to strain with proportionality constant being the dynamic viscosity of the fluid.

On the other hand, turbulent flows are characterized by fluctuations in flow field variables, namely the pressure, density, temperature and velocity in both space and time. Compared to laminar flows as described above, turbulent flows never move in layers and exhibit chaotic behavior. To distinguish between laminar and turbulent flows, a dimensionless number called the Reynolds number is employed. In internal flows such as pipes, the flow becomes turbulent for Reynolds number > 2000 based on diameter of the pipe. The smooth pipe flows at Reynolds < 1500 are laminar and flows in the range 1500 < Re < 2000 are called transitional. The Reynolds number is defined as:

$$\boldsymbol{Re} = \frac{\boldsymbol{ul}}{\boldsymbol{v}} \tag{2-1}$$

2.2 Governing Equations

The governing equations of fluid flow are defined by the three PDEs which describe the conservation of mass, momentum and energy as follows [12]:

Conservation of mass:

$$\frac{\partial \rho}{\partial \mathrm{t}} + \frac{\partial}{\partial x_i}(\rho u_i) = 0 \tag{2.2}$$

Conservation of momentum:

$$\frac{\partial}{\partial t}(\rho u_i) + \frac{\partial}{\partial x_i}(\rho u_i u_j) = -\frac{\partial p}{\partial x_i} + \frac{\partial \tau_{ij}}{\partial x_i} \tag{2.3}$$

Conservation of energy:

$$\frac{\partial}{\partial t}\left[\rho\left(h+\frac{1}{2}{u_i}^2\right)\right]+\frac{\partial}{\partial x_i}\left[\rho u_j\left(h+\frac{1}{2}{u_i}^2\right)\right]=\frac{\partial p}{\partial \mathrm{t}}+\frac{\partial}{\partial x_j}\left(u_i\tau_{ij}+\lambda\frac{\partial T}{\partial x_j}\right) \tag{2.4}$$

Here τ_{ij} is the stress tensor and h is the enthalpy which can be expressed as:

$$\tau_{ij}=\mu\left(\frac{\partial u_i}{\partial x_j}+\frac{\partial u_j}{\partial x_i}\right)-\frac{2}{3}\mu\frac{\partial u_i}{\partial x_i}\,\delta_{ij} \tag{2.5}$$

$$h=C_pT \tag{2.6}$$

2.3 Turbulence Modeling

2.3.1 Reynolds-Averaged Navier-Stokes (RANS) Equations

Navier-Stokes equations given in section 2.2 describe the behavior of unsteady, viscous, heat conducting fluid. In principle they can be solved for turbulent flows by Direct Numerical Simulation (DNS) which does not require any modeling or empiricism or by Large Eddy Simulation (LES)in which only the small scale eddies are modeled. However both these approaches are highly compute intensive and therefore are only used for simulation of flows with simple geometries at low Reynolds numbers. The most widely used approach employed in industrial applications is the time-averaging of Navier-Stokes equations over some time period. The time-averaging results in the so called Reynolds-Averaged Navier-Stokes (RANS) equations which include the so called "Reynolds Stresses" that needs to be modeled. The modeling of "turbulent Stresses" is called "Turbulence Modeling." The incompressible Reynolds-Averaged Navier-Stokes (RANS) equations in time-averaged variables can be expressed as follows:

$$\nabla\cdot\boldsymbol{u}=0 \tag{2.7}$$

$$\rho\left(\frac{\partial \boldsymbol{u}}{\partial t}+\boldsymbol{u}\cdot\nabla\boldsymbol{u}\right)=-\nabla p+(\mu+\mu_t)\nabla^2\boldsymbol{u} \tag{2.8}$$

where $\boldsymbol{u}$ denotes the time-averaged velocity, p the pressure, ρ the density, μ the dynamic viscosity and μ_t the eddy viscosity in the Boussinesq approximation (equivalent to Stokes law for turbulent flow). μ_t is determined by a turbulence model. In the next two sections, we briefly describe the two turbulence models that have been used in this thesis in the numerical simulations.

2.3.2 SST *k-ω* Model

The two-equation SST *k-ω* model [10] is given by the two transport equations: one for *k* and another for ω as follows:

$$\frac{\partial(\rho k)}{\partial t}+\frac{\partial(\rho u_j k)}{\partial x_j}=\hat{P}_k-\hat{D}_k+\frac{\partial}{\partial x_j}\left[(\mu+\sigma_k\mu_t)\frac{\partial k}{\partial x_j}\right] \tag{2-9}$$

$$\frac{\partial(\rho\omega)}{\partial t}+\frac{\partial(\rho u_j\omega)}{\partial x_j}=P_\omega-D_\omega+\frac{\partial}{\partial x_j}\left[(\mu+\sigma_\omega\mu_t)\frac{\partial\omega}{\partial x_j}\right]+2(1-F_1)\frac{\rho\sigma_{\omega2}}{\omega}\frac{\partial k}{\partial x_j}\frac{\partial\omega}{\partial x_j} \tag{2-10}$$

μ_t is the turbulent eddy viscosity which can be expressed as:

$$\mu_t=\frac{\rho a_1 k}{max(a_1\omega,\Omega F_2)} \tag{2-11}$$

Various functions and constants used in the model are given in Reference [10].

2.3.3 Wray- Agarwal Turbulence Model

The latest version of Wray-Agarwal model [11] is a wall-distance free WA2018 model which solves for variable *R* in the following equation:

$$\frac{\partial R}{\partial t}+\frac{\partial u_j R}{\partial x_j}=\frac{\partial}{\partial x_j}\left[(\sigma_R R+\nu)\frac{\partial R}{\partial x_j}\right]+C_1RS+f_1C_{2k\omega}\frac{R}{S}\frac{\partial R}{\partial x_j}\frac{\partial S}{\partial x_j}-(1-f_1)min\left[C_{2k\epsilon}R^2\left(\frac{\frac{\partial S}{\partial x_j}\frac{\partial S}{\partial x_j}}{S^2}\right),C_m\frac{\partial R}{\partial x_j}\frac{\partial R}{\partial x_j}\right] \tag{2.12}$$

The eddy viscosity can be expressed as:

$$\mu_t=\rho f_\mu R \tag{2-13}$$

Various functions and constants used in the model are given in Reference [11].

Chapter 3 Mechanism of Particle Trapping

3.1 Physics of Particle Trapping

To explore why particles can be trapped inside bifurcation pipes, an appropriate fluid-particle force model is needed. There are several fluid-particle interactions based force models in the literature. In most of these models, a single particle experiencing drag, lift, gravity and pressure gradient forces due to fluid is mainly considered. The effects of rotation and near-wall effects are generally neglected at low Reynolds numbers and assuming that most particles keep some distance away from the wall. According to Newton's second law, a force balance model can be written as:

$$\frac{4}{3}\frac{\rho_p}{\rho_f} a \frac{dv}{\mathrm{dt}} = \frac{1}{2}(C_D|u_{rel}|u_{rel} + C_L|u_{rel}|u_{rel} \times \hat{\omega}) - \frac{4}{3} a \nabla p + \frac{4}{3} a \nabla \cdot \tau_f \tag{3.1}$$

Eq. (3.1) is a dimensionless force balance equation with reference quantities D (lateral size or diameter of the pipe) representing the length, U representing the velocity, $U^2\rho$ representing the pressure, and $(LU)^2\rho$ representing the force. Also in Eq. (3.1), a, ρ_p,ρ_f v, and $u_{rel} = u - v$, p and τ_f denote the non-dimensional particle radius, particle density, fluid density, particle velocity, fluid–particle relative velocity, pressure and shear stress on the particle. C_D and C_L respectively denote the drag coefficient and lift coefficient. $\hat{\omega}$ is a unit vector describing the direction of vorticity vector.

Lift force on a particle can be contributed by inertia [13-14] as well as by deformation. According to Vigolo's study [1], the deformation of particle has almost no influence on the results. Therefore, considering only the inertial lift force, the simulation in this thesis adopted the lift model of Kurose and Komori [13].

Through detailed simulation with the software LIGGGHTS, Vigolo [1] found that drag and pressure-gradient compete with each other in the radial direction, while the influence of lift and viscous stresses is too small and can be ignored. These are reasonable assumptions since the results show that the slip velocity between fluid and particle is small enough. Even at high fluid Reynolds number, the typical particle Reynolds number is much smaller than 1. Other advanced lift model also show similar result

showing that the lift force is negligible, since these models also depend on the particle Reynolds number.

It has also been shown that the forces in the tangential direction are also negligible. Finally, considering all forces acting on the particle, it can be concluded that when a particle gets trapped, the pressure-gradient force in the vortex core is completely balanced by the drag force which acts in the opposite direction. Thus the physics of particle trapping can be mainly attributed to the balance between the pressure-gradient force and drag force.

3.2 Theoretical Model of Force Balance

Based on the considerations presented in section 3.1, we only consider drag forces and pressure-gradient forces to study the force balance of the trapped particles. Thus, neglecting lift, viscous stresses and other forces, the force balance equation in the axial direction in the pipe can be written as:

$$\frac{4}{3}\frac{\rho_p}{\rho_f} a \frac{dv}{\mathrm{dt}} = \frac{C_D}{2}|u_{rel}|u_{rel} - \frac{4}{3} a \nabla p + \frac{4}{3} a \frac{\rho_p}{\rho_f}(|\Omega|^2 r - 2\Omega \times \boldsymbol{v}) \tag{3.2}$$

In Eq. (2), Ω represents the non-dimensional rotational velocity around the vortices. The velocities in this equation are the velocities relative to the rotating coordinate system. The last term is the sum of centrifugal and Coriolis force. Similarly, we can also write the radial force balance equation as:

$$\frac{4}{3}\frac{\rho_p}{\rho_f} a\ddot{r} = \frac{C_D}{2} u_r^2 - \frac{4}{3} a \left(\frac{\partial \mathrm{p}}{\partial \mathrm{r}} - \frac{\rho_p}{\rho_f}\frac{u_\phi^2}{r}\right) \tag{3.3}$$

A critical value of a can be deduced noting that the particle radius must be larger than the radius of the vortex core so that the particles have a chance to get away from the vortex core. Particle density plays an important role in the force balance in the radial direction. When $\frac{\rho_p}{\rho_f}$ reaches certain value, the critical particle diameters can be very large and all particles can leave the vortex core and thus no particle trapping will occur.

3.3 Particle Trapping Probability

According to Vigilo et al. [1], flow reversal happens when Reynolds number is higher than 350. Then permanent particle trapping can happen, and a certain percentage of particles released can be trapped in the vortex core permanently. They showed that fluid Reynolds number, particle diameter and particle-fluid density ratio all have a big influence in particles entering or leaving the vortex core. This thesis studies the influence of Reynolds number and particle diameters by numerical simulation; the computed results match the predictions of Vigilio et al. quite well. This thesis also investigates the influence of bifurcation angle. It is found that the probability of particle trapping and its rate increases as the bifurcation angle decreases from 90^{o} and becomes negligible as the bifurcation angle increases from 90^{o}. This is a very important result which has never been reported in the previous literature.

Chapter 4 Particle Trapping in T-junction Flow

4.1 Mechanisms of Particle Trapping in T-junction at Low Reynolds Numbers

4.1.1 Overview

Based on Vigolo et al.'s work [1], it can be inferred that Reynolds number is the main parameter that influences the particle trapping irrespective of the size and other geometric parameters of the T-junction. In this section, we consider a T Junction geometry with both inlet and outlet of circular cross-section. The diameters of both inlet and outlet pipes are 2 cm and lengths of the pipes are 20 cm. 3D models were established in SOLIDWORKS and meshed as blocks with structured grids using ICEM-CFD as shown in Figure 4.1 Compared to unstructured grids, structured grids have the advantages of fast generation, high quality and simple data structure. In Figure 4.2, the region of boundary layer is also refined to maintain the accuracy of the calculation. The total number of hexahedral cells is 1,097,354.

(A)

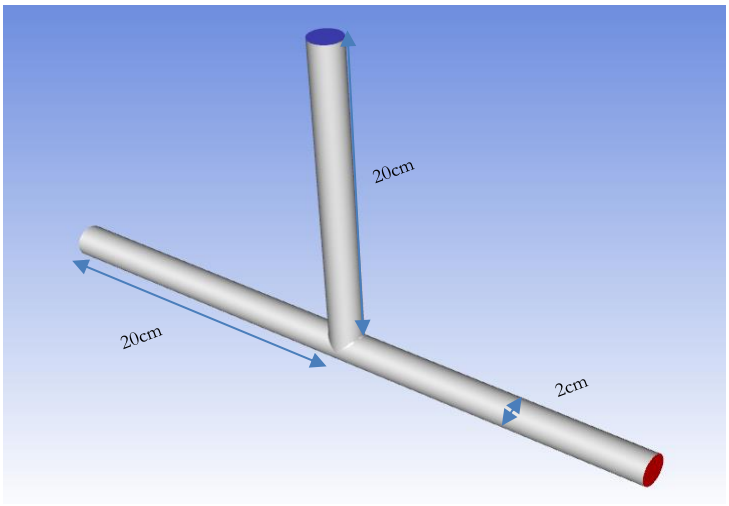

(B)

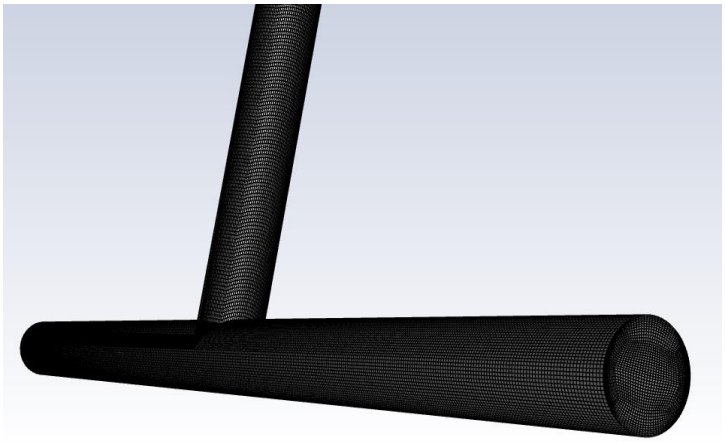

Figure 4.1: (A) Geometry of T-Junction with Circular Cross-section & (B) Structured Grids inside T-Junction

(A)

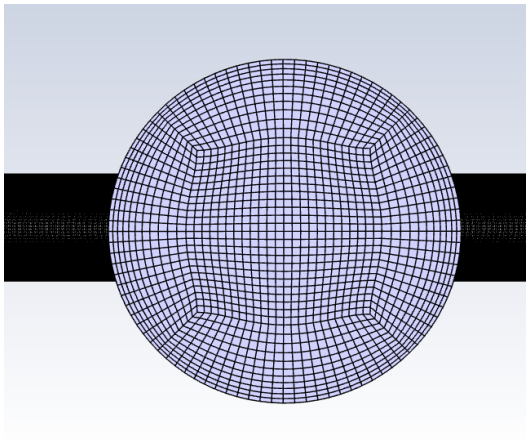

(B)

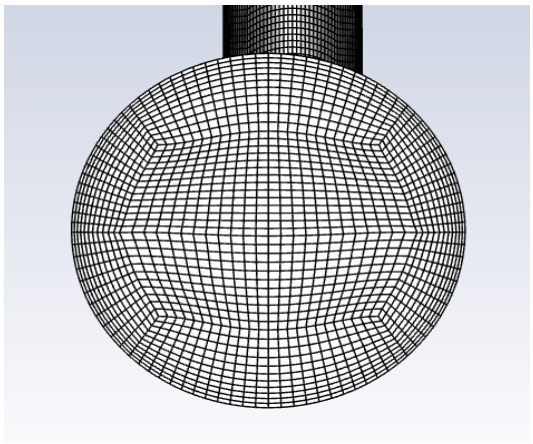

Figure 4.2: Refined Boundary Layer in (A) Inlet Pipe & (B) Outlet Pipe

To analyze laminar flow, velocity profile at the inlet is considered to be parabolic with maximum centerline value of 0.03618 (m/s) which is two times the average velocity. The velocity profile for Re = 360 is shown in Figure 4.3.

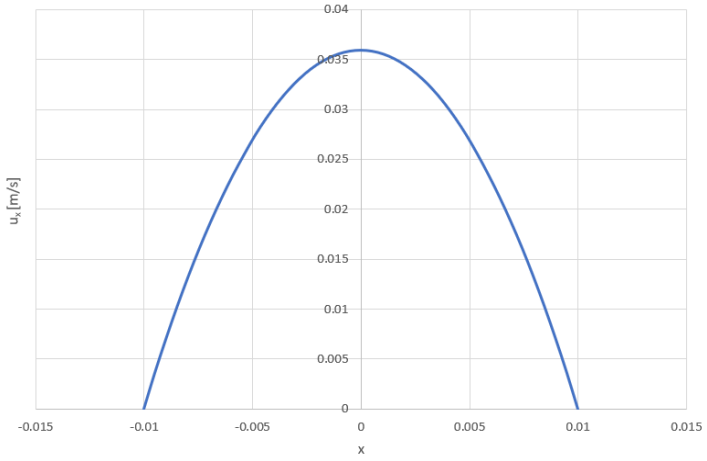

Figure 4.3: Parabolic Velocity Profile at Inlet

The Contours of velocity, pressure, wall-shear stress, and streamlines are shown in Figure 4.4.

(A)

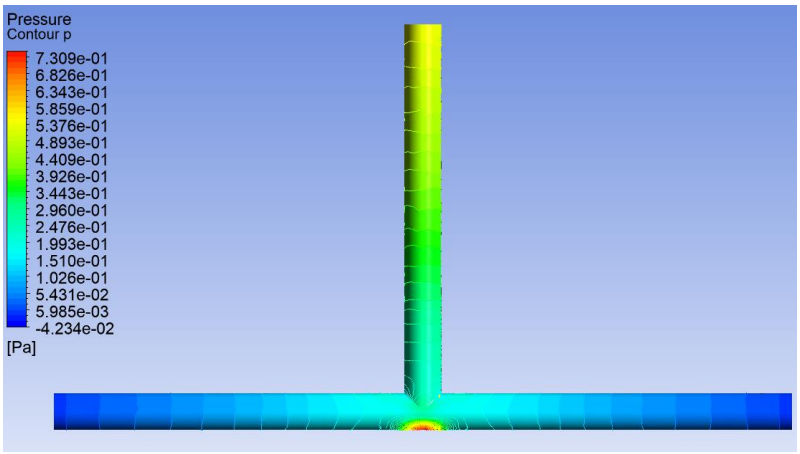

(B)

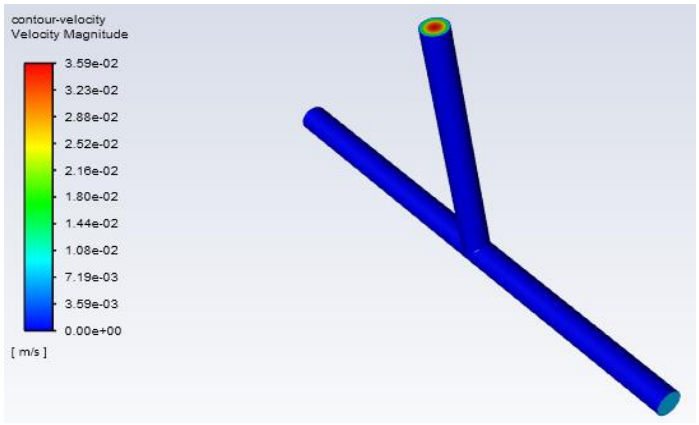

(C)

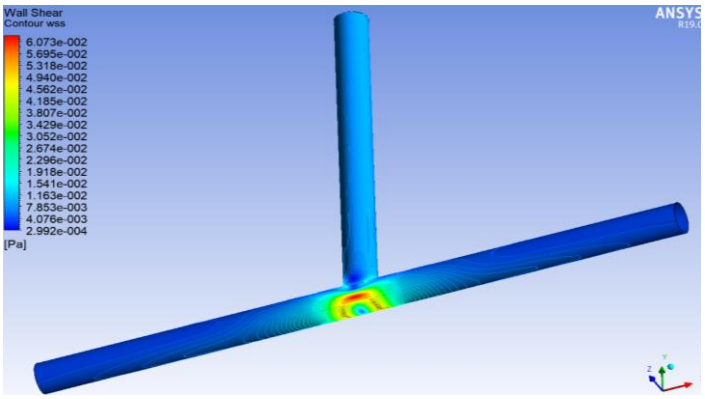

(D)

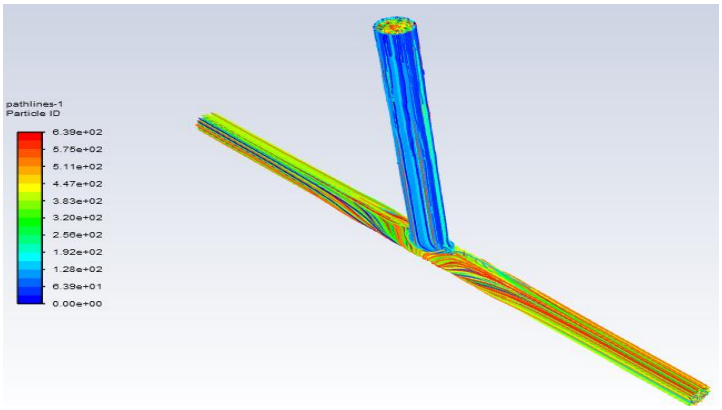

Figure 4.4: (A) Pressure Contours, (B) Velocity Contours, (C) Wall Shear Stress Contours,and (D) Streamlines in T- Junction Flow (Re = 360)

Figure 4.5 shows the variation in axial pressure gradient with x along the vortex core line at Re = 360.

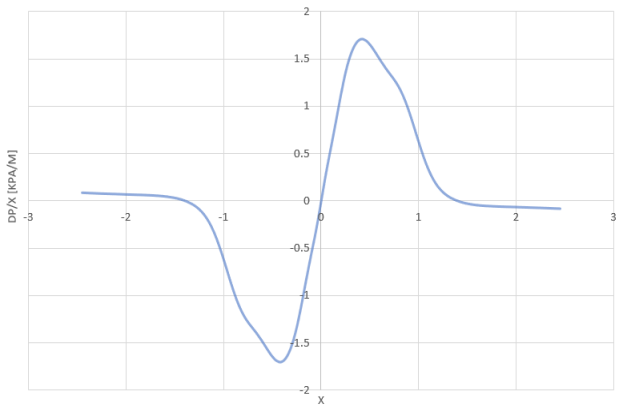

Figure 4.5: Axial Pressure Gradient along Vortex Core Line

4.1.2 Influence of Particle Diameter in Particle Trapping

For particle injection, 1632 particles are released from the inlet with the local fluid velocity. The particles are considered to be of uniform diameter D_p =0.01 mm, 0.1 mm, 1 mm and 2 mm with density = 150kg/m^3 which is 15% of the density of water. Particle flow rate is fixed at 10^{-6} kg/s. The graphs of particle tracking for different particle diameters are shown in Figure 4.6.

(A) D_p = 0.01 mm

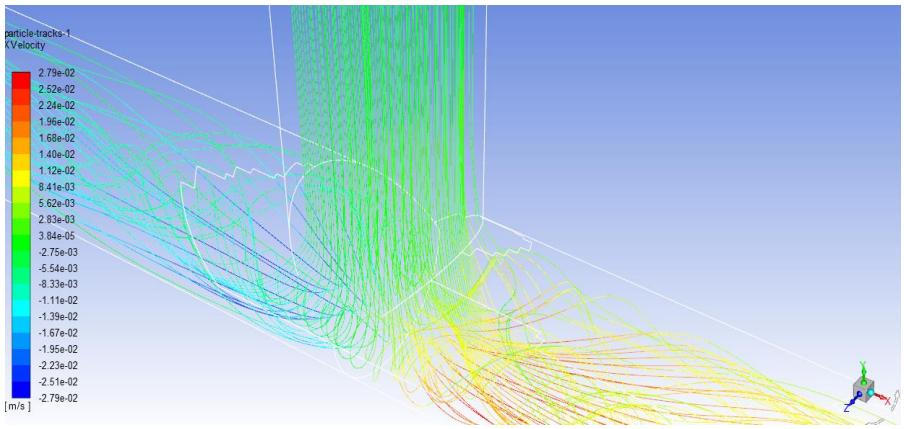

(B) D_p = 0.1 mm

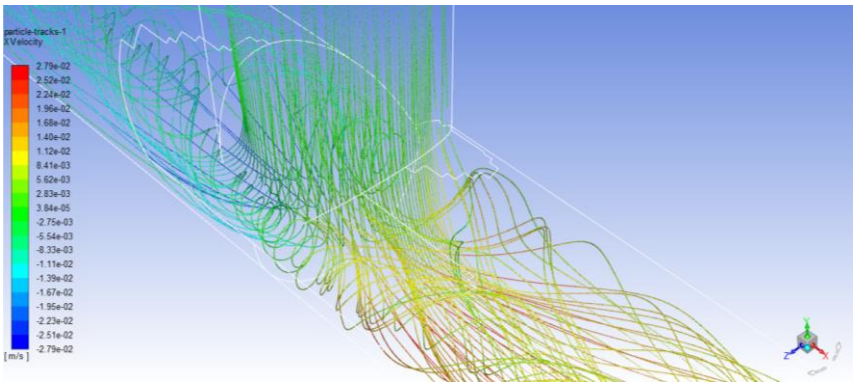

(C) D_p = 1 mm

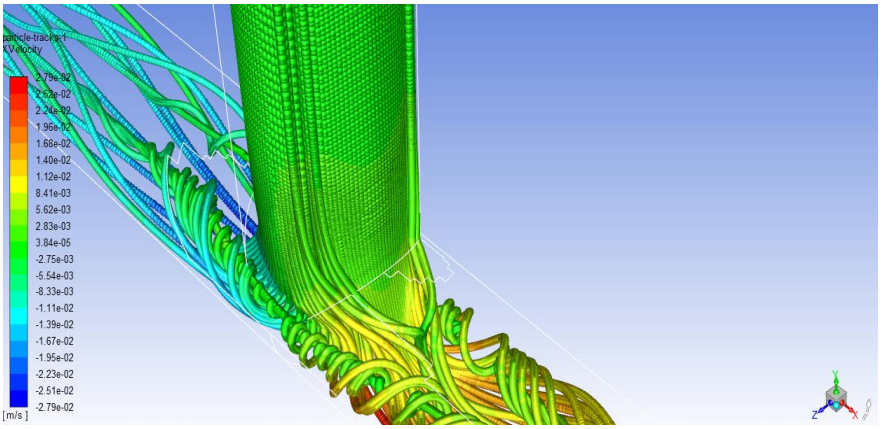

(D) D_p = 2 mm

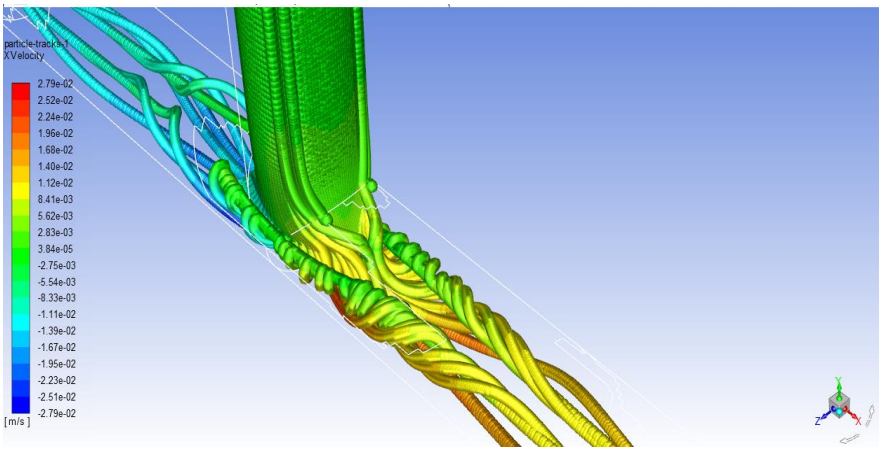

Figure 4.6: Particle Tracking of Different Particle Diameters in T-Junction (Re = 360)

It can be noticed from Figure 4.6 (A) and (B) that no particle is trapped in the vortex core. The small particles rotate keeping some distance from the core line. But when D_p is increased to 1mm which is

5% of the inlet diameter, some particles get trapped in the vortex line and form a particle chain inside the vortices. When D_p = 2 mm, particle trapping is more obvious as shown in Figure 4.6 (D). The percentage of particles trapped increases from 31.07% (507/1632) to 55.2% (898/1632) when particle diameter is increased from 1 mm to 2 mm.

All case studies were computed in a pressure-based CFD solver in Fluent with the transitional turbulence model k-kl-omega. A coupled scheme was used to solve pressure and momentum equations simultaneously. PRESTO! pressure interpolation, Green-Gauss node-based gradient scheme, and second-order upwind schemes for momentum and turbulent kinetic energy were chosen. Each case converged to a residual value of 10^{-6} and continued until 1000 time step iterations were achieved. Several pressure, velocity, and average WSS monitors were employed, recording data at every time step to insure proper convergence.

Once each calculation was complete, data was extracted within the solver through the reports tab. Reports for facet average/minimum/maximum WSS as well as volumetric flow rate for both PA exits were taken. All post processing was done in ANSYS CFD Post. Several WSS and velocity contour plots were created for each computed case.

4.1.3 The Influence of Reynolds Number in Particle Trapping

To explore the influence of Reynolds number in particle trapping, we chose to fix the particle diameter to 1 mm and changed the Reynolds number from 150 to 480. It is shown in Figure 4.7 that no trapping occurs at Re = 150 and 250, and most particles get trapped at Re = 480 compared to other low Reynolds number cases.

(A)

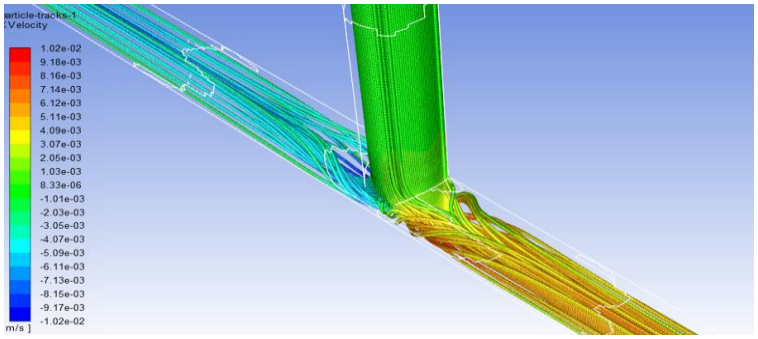
article-tracks-1
Velocity
1.02e-02
9.18e-03
8.16e-03
7.14e-03
6.12e-03
5.11e-03
4.09e-03
3.07e-03
2.05e-03
1.03e-03
8.33e-06
-1.01e-03
-2.03e-03
-3.05e-03
-4.07e-03
-5.09e-03
-6.11e-03
-7.13e-03
-8.15e-03
-9.17e-03
-1.02e-02
m/s]

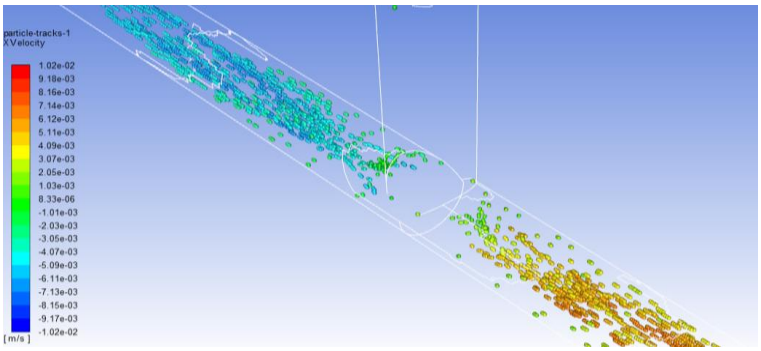
particle-tracks-1
XVelocity
1.02e-02
9.18e-03
8.16e-03
7.14e-03
6.12e-03
5.11e-03
4.09e-03
3.07e-03
2.05e-03
1.03e-03
8.33e-06
-1.01e-03
-2.03e-03
-3.05e-03
-4.07e-03
-5.09e-03
-6.11e-03
-7.13e-03
-8.15e-03
-9.17e-03
-1.02e-02
[m/s]

(B)

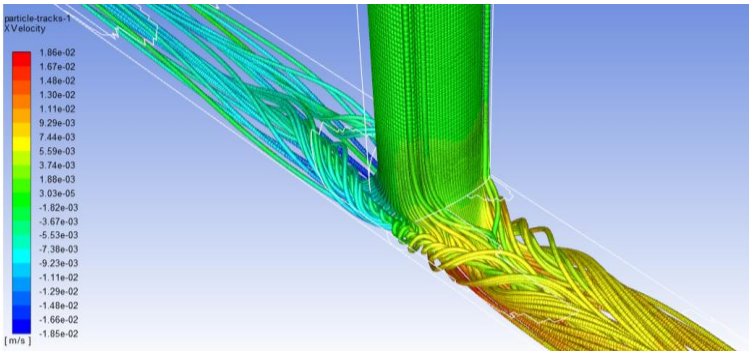
particle-tracks-1
XVelocity
1.86e-02
1.67e-02
1.48e-02
1.30e-02
1.11e-02
9.29e-03
7.44e-03
5.59e-03
3.74e-03
1.88e-03
3.03e-05
-1.82e-03
-3.67e-03
-5.53e-03
-7.38e-03
-9.23e-03
-1.11e-02
-1.29e-02
-1.48e-02
-1.66e-02
-1.85e-02
[m/s]

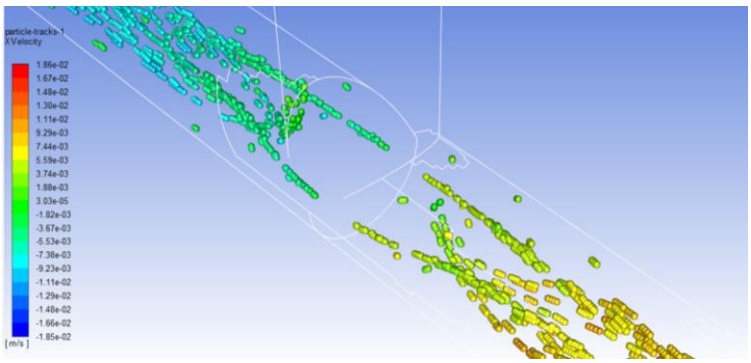
particle-tracks-1
XVelocity
1.86e-02
1.67e-02
1.48e-02
1.30e-02
1.11e-02
9.29e-03
7.44e-03
5.59e-03
3.74e-03
1.88e-03
3.03e-05
-1.82e-03
-3.67e-03
-5.53e-03
-7.38e-03
-9.23e-03
-1.11e-02
-1.29e-02
-1.48e-02
-1.66e-02
-1.85e-02
[m/s]

(C)

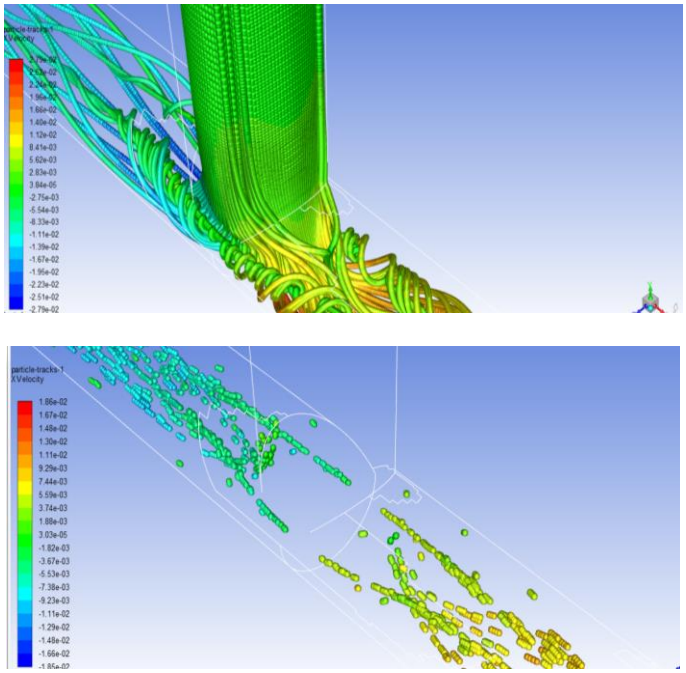

(D)

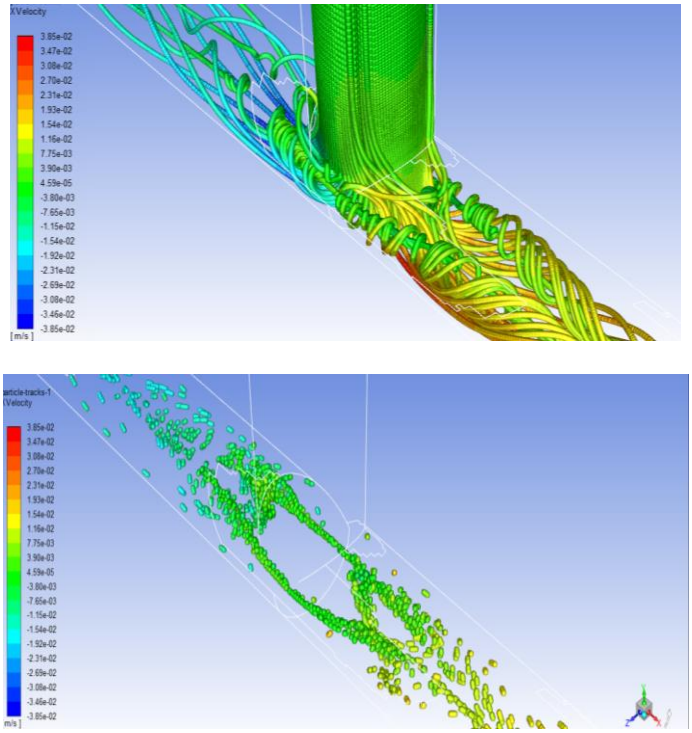

Figure 4.7: Particle Trapping at Different Reynolds Numbers in T-Junction at Re = (A) 150, (B) 250, (C) 360 and (D) 480

It can be noticed that no particle can get inside the vortex core until Reynolds number increases to 250. Also, the particle trapping is not permanent: the particles at the vortex core move slowly and finally escape from the outlet. Detailed simulations show that the permanent particle trapping only happens when Re > 350. And the increase in Reynolds number can also increase the percentage of particles trapped. About 50.06% of particles (817/1632) get trapped in the case of Re = 480, while only 31.07% of them (507/1632) get trapped when Re =360.

4.2 Mechanisms of Particle Trapping in T-Junction at High Reynolds Number

In this section, we again consider the circular cross-section geometry of T-junction and set inlet boundary condition as the mass-flow inlet with flow rate of 0.04726kg/s. Reynolds number is about 3,000 which results in turbulent flow. We consider SST k-ω and WA turbulence models [10] to solve the Reynolds-Averaged Navier-Stokes (RANS) equations. The computations of pressure, velocity, wall shear stress contours and streamlines are shown in Figure 4.8.

(A)

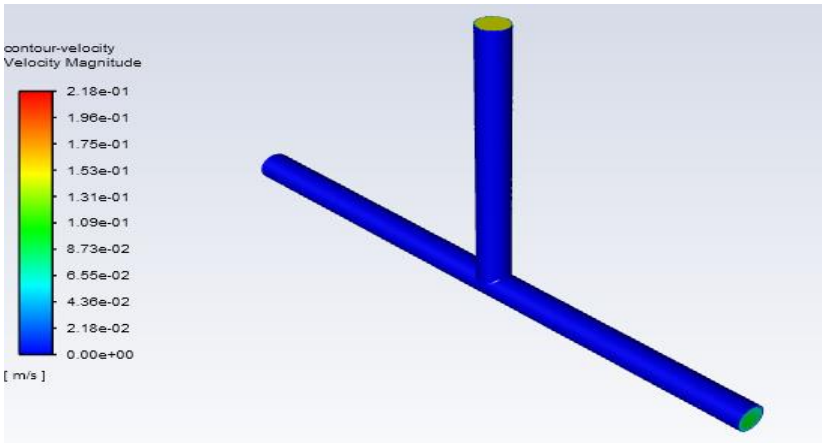

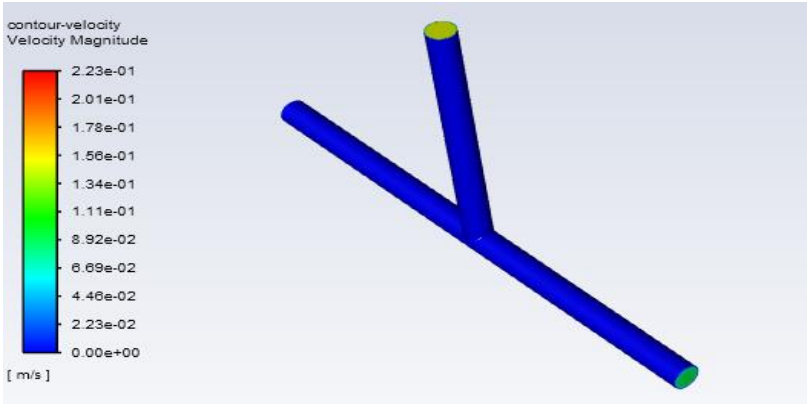

(B)

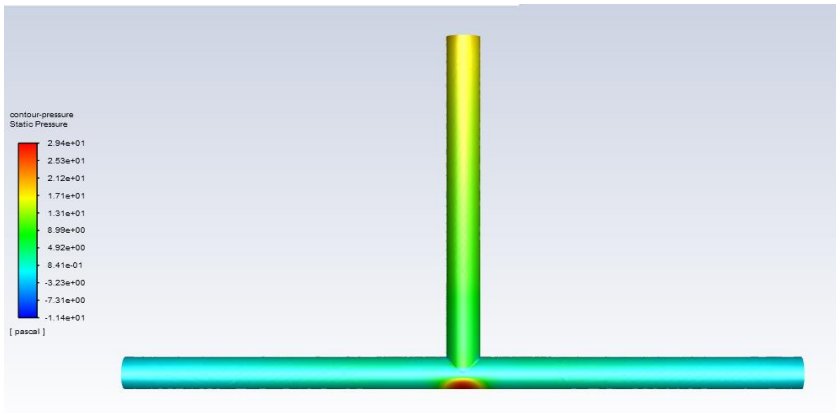
contour-pressure
Static Pressure
2.94e+01
2.53e+01
2.12e+01
1.71e+01
1.31e+01
8.99e+00
4.92e+00
8.41e-01
-3.23e+00
-7.31e+00
-1.14e+01
[pascal]

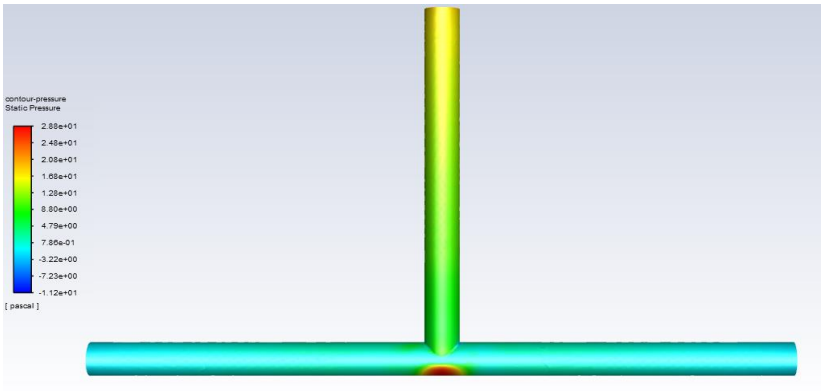
contour-pressure
Static Pressure
2.88e+01
2.48e+01
2.08e+01
1.68e+01
1.28e+01
8.80e+00
4.79e+00
7.86e-01
-3.22e+00
-7.23e+00
-1.12e+01
[pascal]

(C)

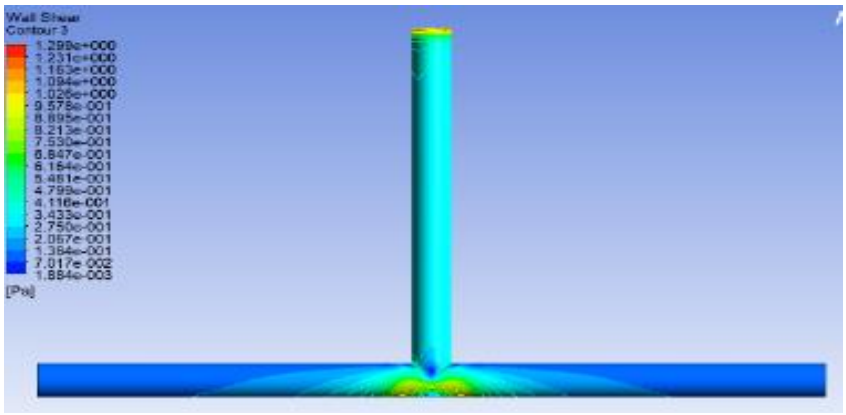
Wall Shear
Contour 3
1.298e+000
1.231e+000
1.163e+000
1.094e+000
1.026e+000
9.578e-001
8.895e-001
8.213e-001
7.530e-001
6.847e-001
6.164e-001
5.481e-001
4.799e-001
4.116e-001
3.433e-001
2.750e-001
2.067e-001
1.384e-001
7.017e-002
1.884e-003
[Pa]

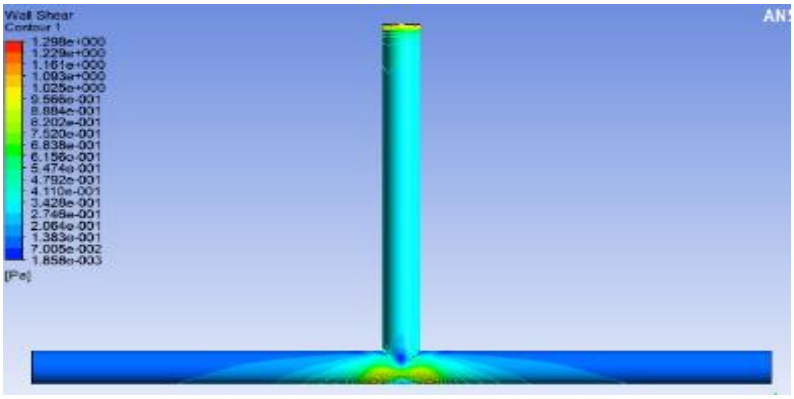
Wall Shear
Contour 1
1.298e+000
1.229e+000
1.161e+000
1.093e+000
1.025e+000
9.566e-001
8.884e-001
8.202e-001
7.520e-001
6.838e-001
6.156e-001
5.474e-001
4.792e-001
4.110e-001
3.428e-001
2.746e-001
2.064e-001
1.383e-001
7.005e-002
1.858e-003
[Pa]

(D)

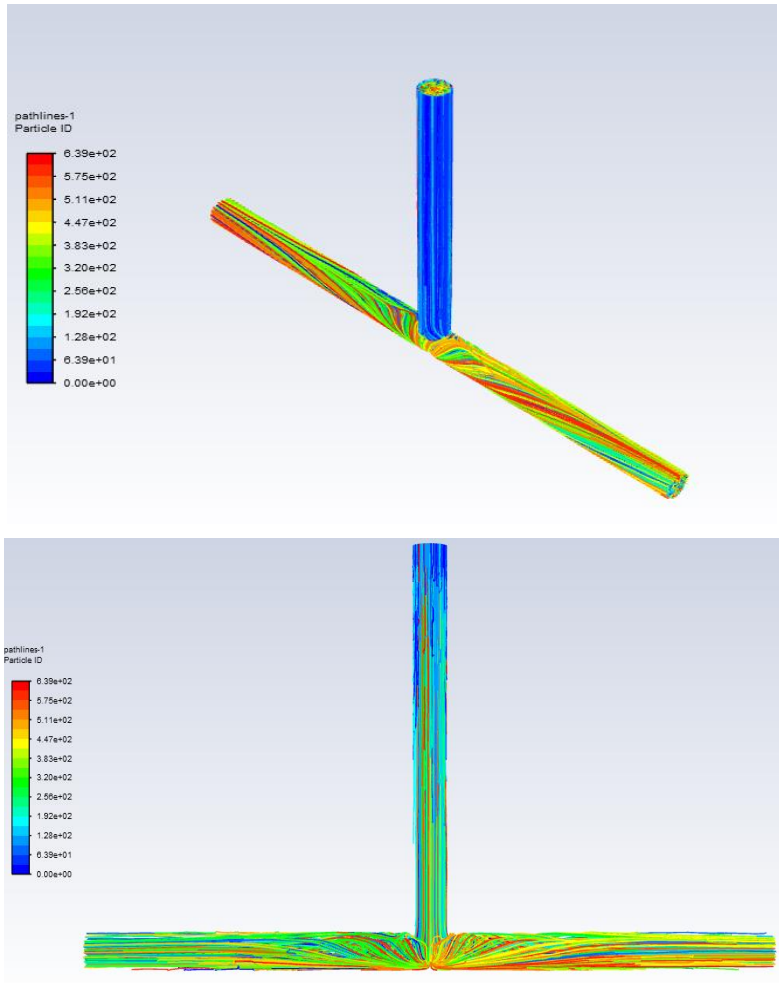

Figure 4.8: (A) Pressure Contours, (B) Velocity Contours, (C) Wall Shear Stress Contours & (D) Streamlines for Turbulent Flow (Top are Results from SST Model and Bottom are from WA Model)

Numerical simulations show that both SST k-ω and Wray-Agarwal (WA) turbulence models give similar results as shown in Figure 4.9. The differences in solutions of SST k-ω and Wray-Agarwal (WA) turbulence models in highest axial velocity and pressure gradient are no more than 8.5% and 2.7% respectively. Experimental results are needed for validation and verification. The particles distribution/trapping shown in Figure 4.10 is totally different from that in laminar flow and no particle is trapped in the vortex core.

(A)

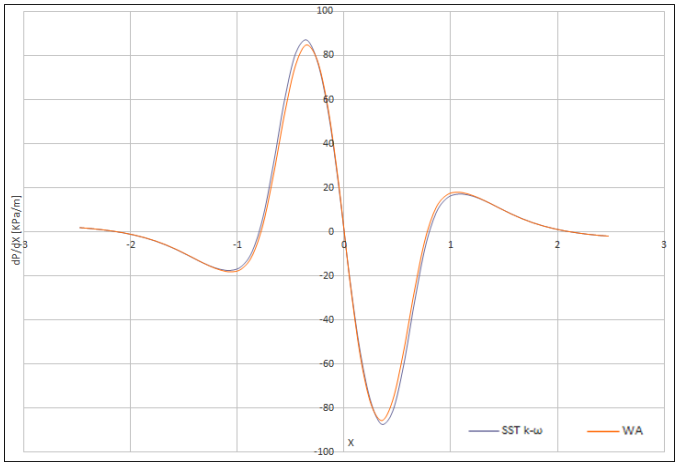

(B)

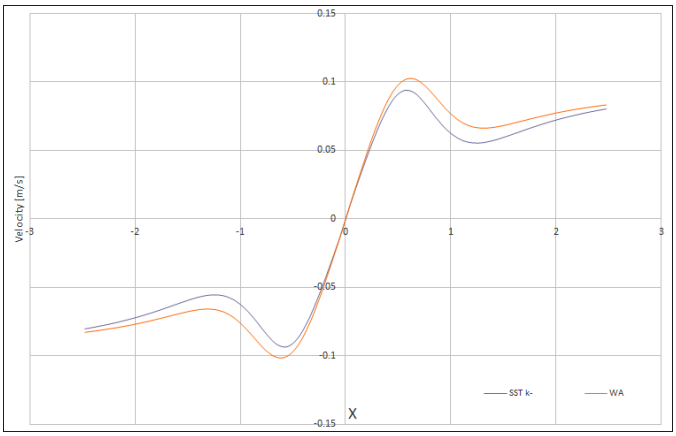

Figure 4.9: (A) Pressure Gradient and (B) Axial Velocity in The Vortex Core Line in Turbulent T-Junction Flow Using SST k-ω and Wray-Agarwal Turbulence Models

(A)

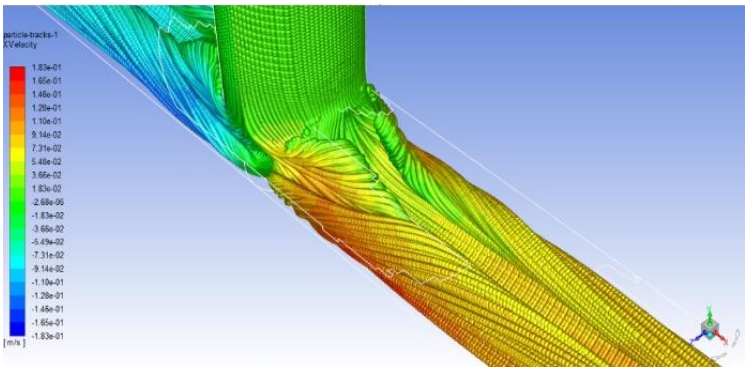

(B)

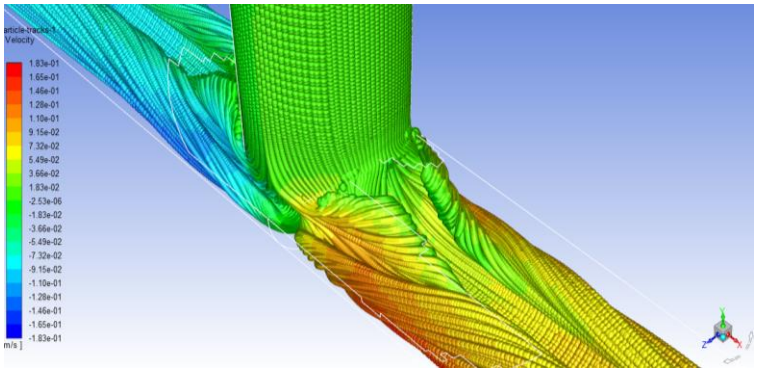

Figure 4.10: Particle Trapping for Re = 3000 Using (A) SST Model and (B) WA Model

3.4 Validation

The validation model of T-junction flow is created according to the size in the experiment of Vigolo et al.'s [1]. Their experimental device has 1 inlet and 2 outlets with square cross-section with each side of 4 mm. The axial lengths of all three pipes are 40 mm as shown in Figure 4.11. An optimized mesh method is applied to the model with lateral length and pipe length having a division number of 40 and 400 respectively. To improve the accuracy of the calculation, the boundary layer region is refined smoothly with a bias factor of 1.2 as shown in Figure 4.12. The number of grid nodes is 2,063,801, which are found to be sufficient to obtain a mesh independent solution.

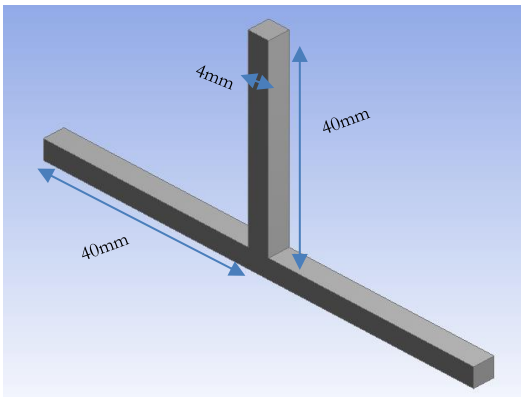

Figure 4.11: Physical Model for CFD Validation Study (T-Junction with Pipes of Square Cross-Section)

(A)

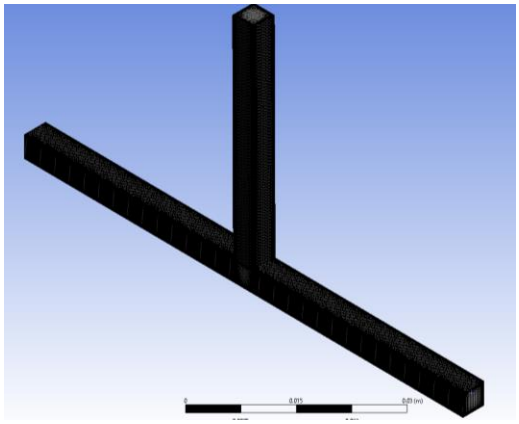

(B)

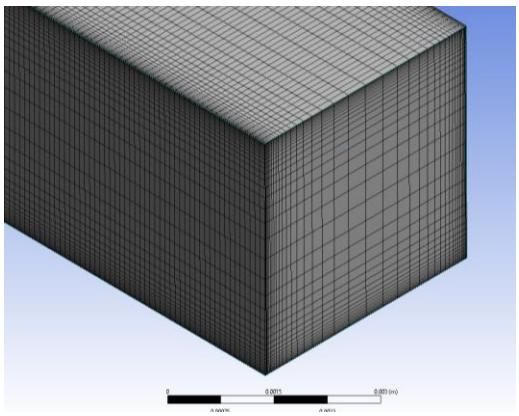

Figure 4.12: (A) Mesh and (B) Refined Boundary Layer Region of the T-Junction

For boundary conditions, the inlet is set as the mass-flow-inlet with flow rate ranging from 6.018×10-4 kg/s to 1.003×10-3 kg/s with the average velocity ranging from 0.03768 m/s to 0.0628 m/s. Flow direction is set towards the negative direction of y- axis. Boundary conditions on the two outlets are pressure-outlet with gauge pressure of 0. No slip condition is used at all walls. The material of the fluid is water with density of 998.2kg/m^3 and viscosity of 0.001003kg/ (m· s).

Figure 4.13 shows the streamlines inside the T-junction when Re=150. The flow field clearly shows two symmetric vortices in the junction area; colors indicate the magnitude of velocity. To achieve validation and verification, data for pressure gradient along the vortex core line is considered. The vortex core is determined as the point of local minimum pressure in Y-Z cross section where X is non-dimensional coordinate defined as x/L. The computed axial pressure gradients along the vortex core line are shown in Figure 4.14.

(A)

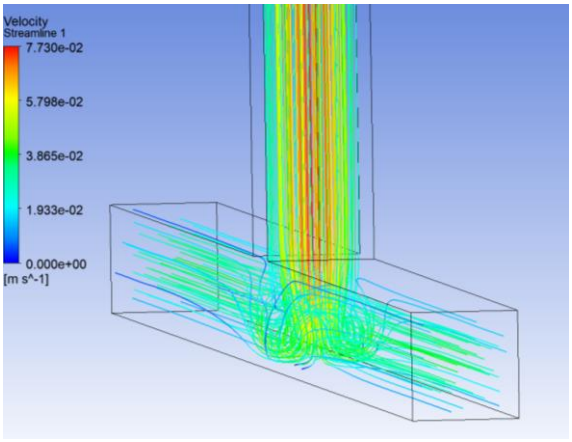

(B)

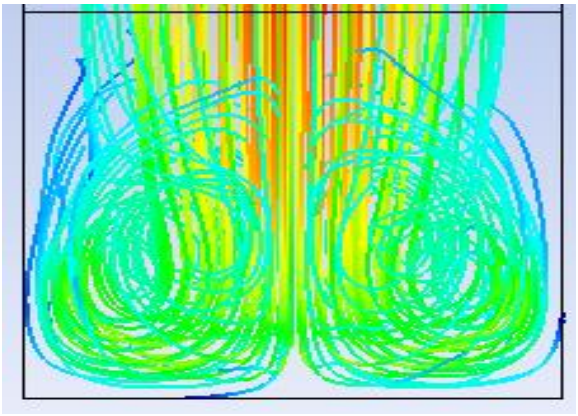

Figure 4.13: (A) Streamlines and (B) Vortex Structure for Re = 150

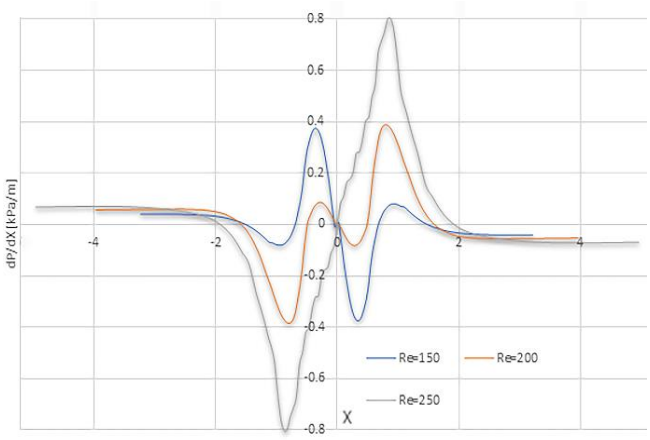

Figure 4.14: Axial Pressure Gradient Versus X Position for Re = 150, 200 and 250

Figure 4.15 shows the experimental results for axial pressure gradient with x position for Re = 150, 200 and 250. Comparing the graphs in Figure 4.14 and Figure 4.15, it can be noticed that the simulation results match the experimental data quite well and both numerical and experimental results indicate a shift in the pressure gradient when Re is between 200 and 250. Small difference in the results in two figures may be attributed to differences in determining the position of the vortex core line.

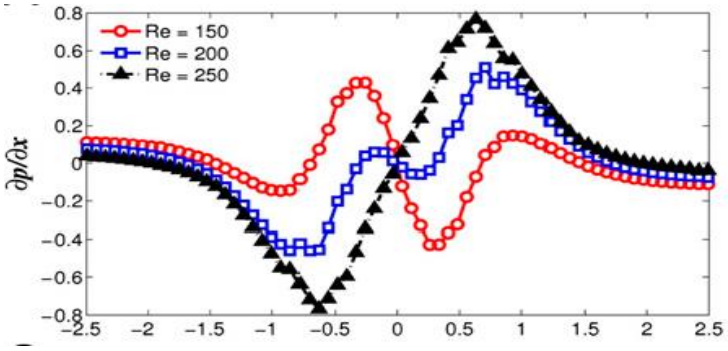

Figure 4.15: Variation in Axial Pressure Gradient with X Along the Vortex Core Line [1]

Chapter 5 Particle Trapping in Y-junction Flows

5.1 Mechanisms of Particle Trapping in T-junction Flow at Low Reynolds Numbers

5.1.1 Overview

The model used in this section is shown in Figure 5.1. All pipes are straight having a uniform diameter of 2 cm and length of 20 cm. The angle between 2 daughter pipes is 90°. The average Reynolds number at the inlet is 360 and all other setup is the same as in the case of T-junction flow in chapter 4 with pipes of square cross-section.

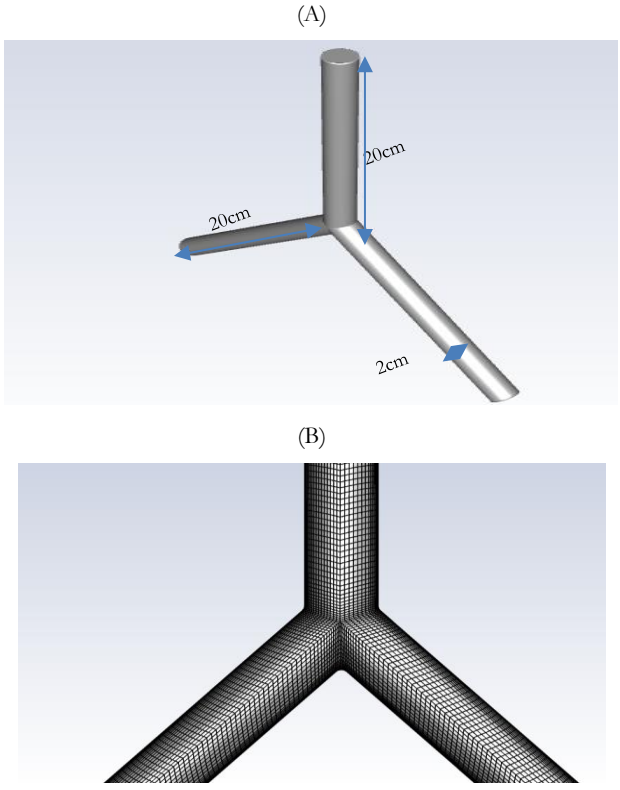

Figure 5.1: (A) Geometry and (B) Mesh inside Y-Junction

The contours of pressure, velocity, wall shear stress and streamlines are as shown in Figure 5.2.

(A)

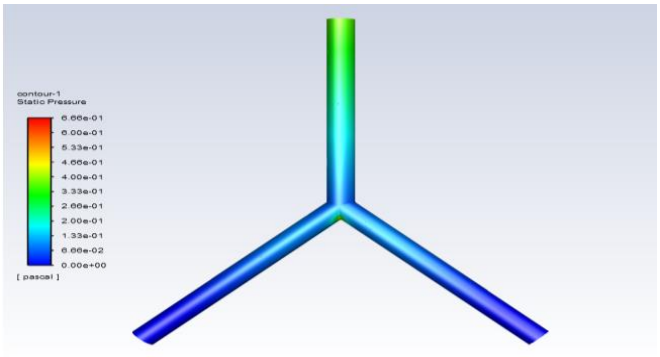
contour-1
Static Pressure
6.66e-01
6.00e-01
5.33e-01
4.66e-01
4.00e-01
3.33e-01
2.66e-01
2.00e-01
1.33e-01
6.66e-02
0.00e+00
[pascal]

(B)

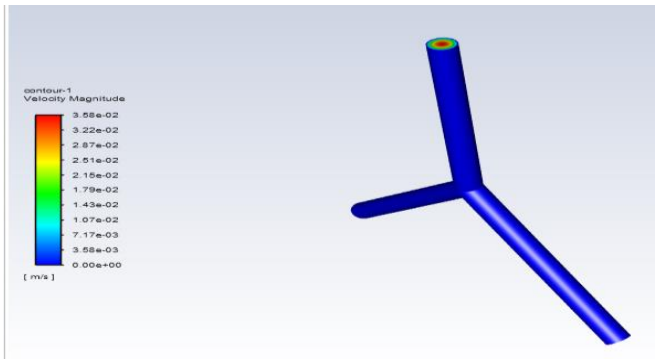
contour-1
Velocity Magnitude
3.58e-02
3.22e-02
2.87e-02
2.51e-02
2.15e-02
1.79e-02
1.43e-02
1.07e-02
7.17e-03
3.58e-03
0.00e+00
[m/s]

(C)

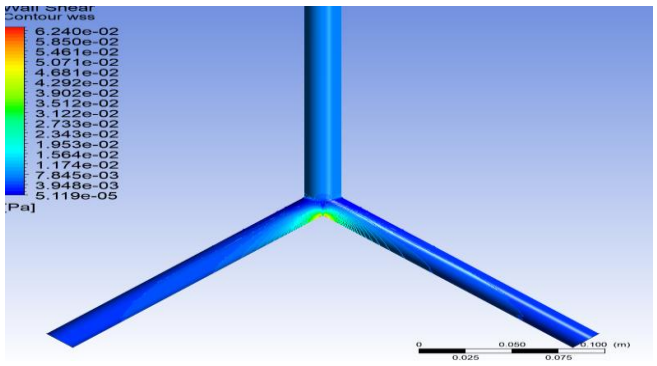
Wall Shear
Contour was
6.240e-02
5.850e-02
5.461e-02
5.071e-02
4.681e-02
4.292e-02
3.902e-02
3.512e-02
3.122e-02
2.733e-02
2.343e-02
1.953e-02
1.564e-02
1.174e-02
7.845e-03
3.948e-03
5.119e-05
[Pa]
0
0.050
0.100 (m)
0.025
0.075

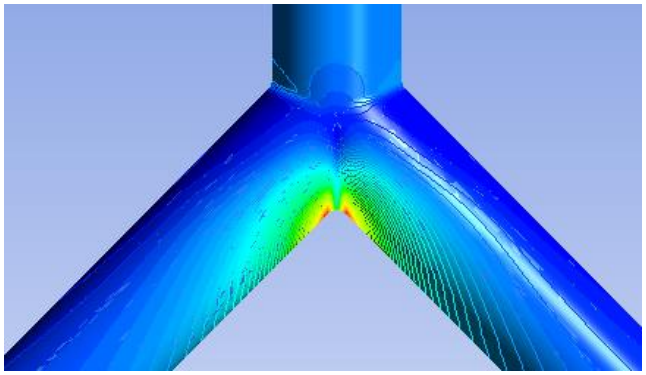

(D)

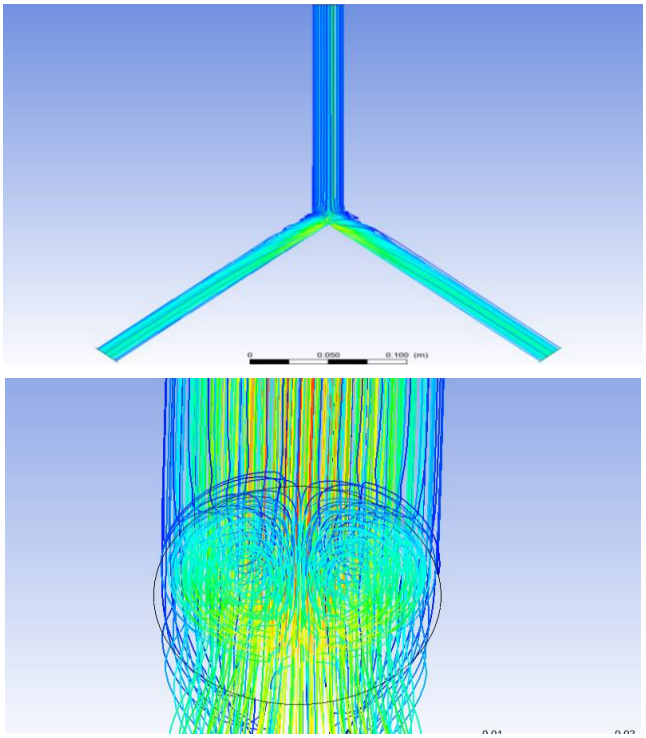

Figure 5.2: (A) Pressure Contours, (B) Velocity Contours, (C) Wall Shear Stress Contours and (D) Streamlines in Y-Junction Laminar Flow

To study the mechanism of particle trapping in Y-junction laminar flow, we increase the Reynolds number from 360 to 420, 480 and 520. As the Reynolds number is increased, no particle trapping is observed as shown in Figure 5.3. Further study about particle trapping in Y-junction flow is needed.

(A)

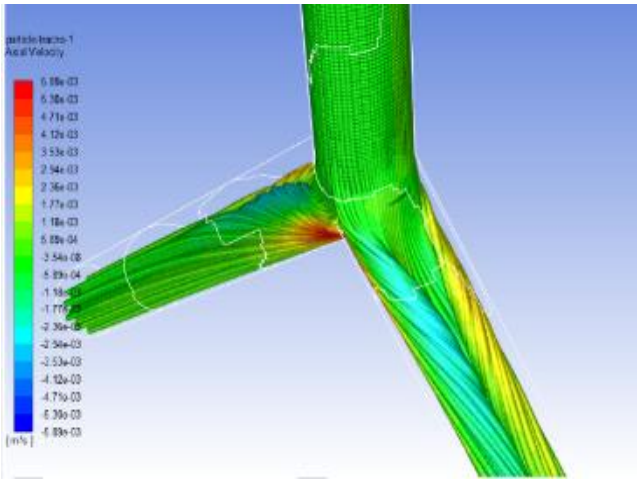

(B)

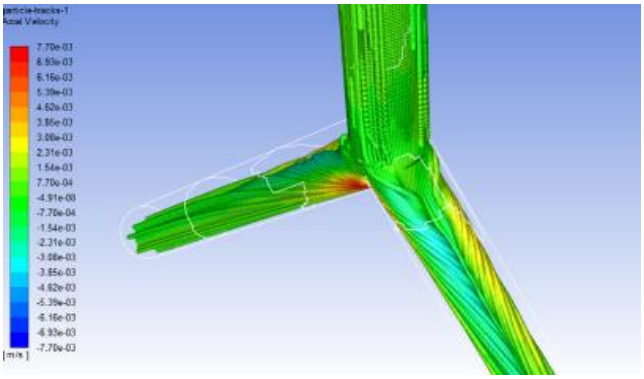

(C)

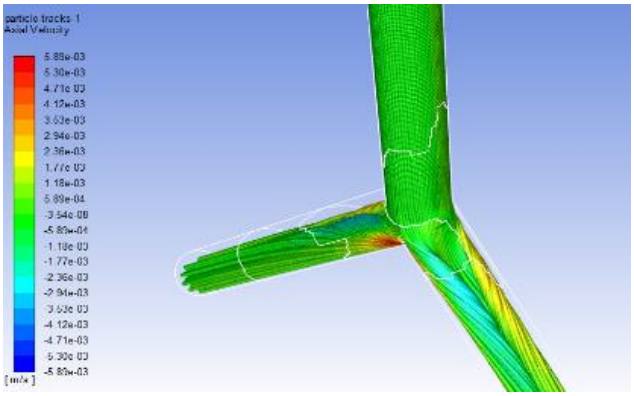

(D)

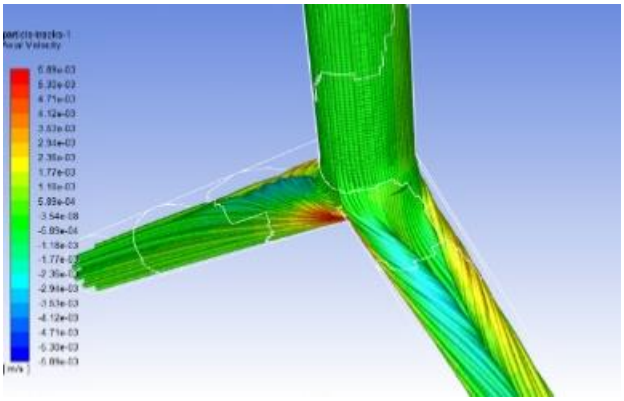

Figure 5.3: Particle Trapping in Y- Junction Flow at Re = (A) 360, (B) 420, (C) 480 and (D) 540

5.1.2 Y-Junction Flow with Stenosis

To investigate the influence of stenosis near Y-junction, we add a stenosis at the entrance of one daughter pipe of the Y-junction model. The stenosis has a length of 2 cm and height of 0.5 cm. Its shape is an arc with radius of 2 cm. The geometry of the bifurcation and stenosis is shown in Figure 5.4.

(A)

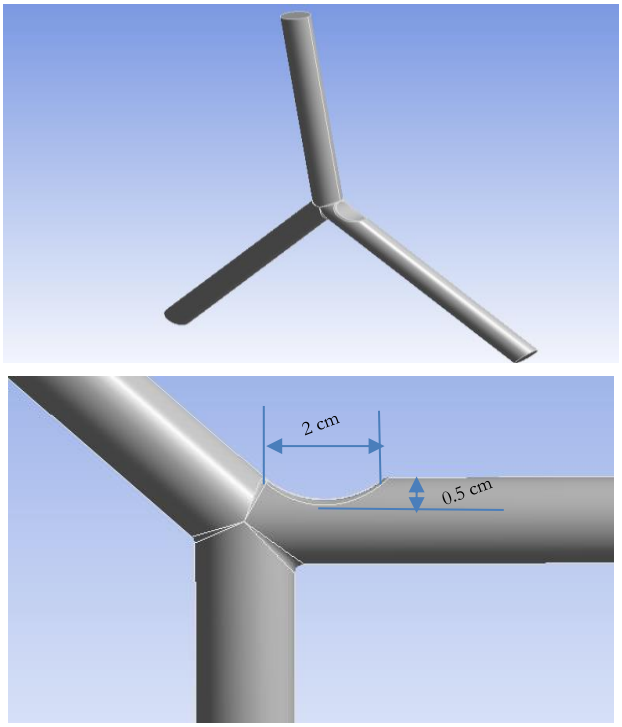

(B)

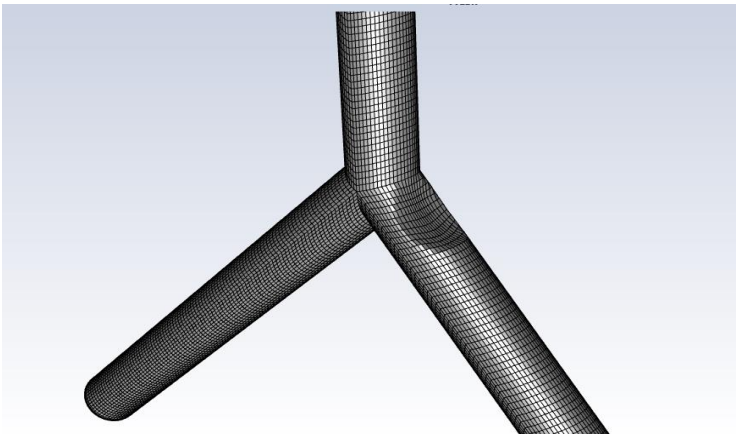

Figure 5.4: (A) Geometry and (B) Mesh in the Bifurcation Model with Stenosis

Figure 5.5 and Figure 5.6 include several plots of velocity and vorticity distribution in different Y-junction models. The plots are equally spaced normal to the flow direction. It can be seen that the stenosis has much more impact on vorticity than on velocity magnitude. The maximum value of vorticity after the bifurcation is about 36/s in the model with stenosis while the maximum vorticity in

the normal bifurcation without stenosis is not more than 23/s. The largest velocity in the two models after bifurcation is about 0.031 m/s. These results are close to the simulation results of Antonova [9].

(A)

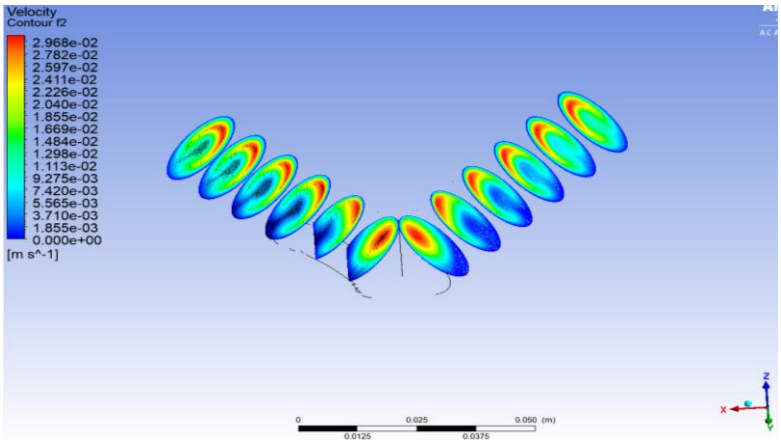

(B)

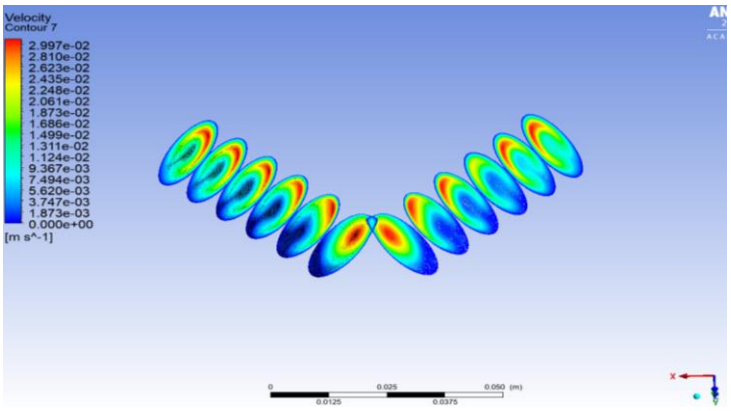

Figure 5.5: Velocity Distribution at Various Pipe Cross – Sections in Y-Junction Flow, (A) with and (B) without Stenosis

(A)

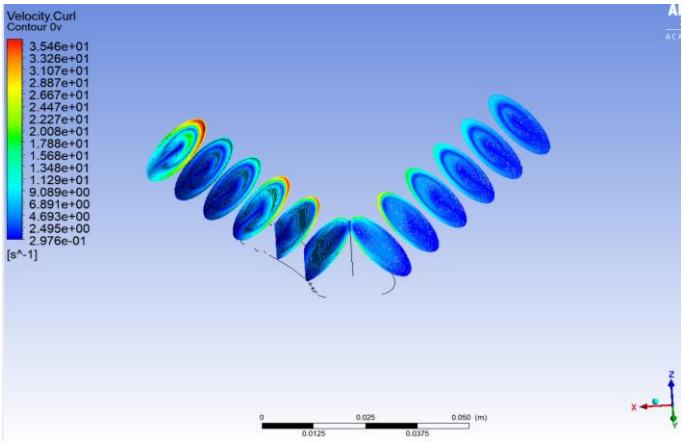

(B)

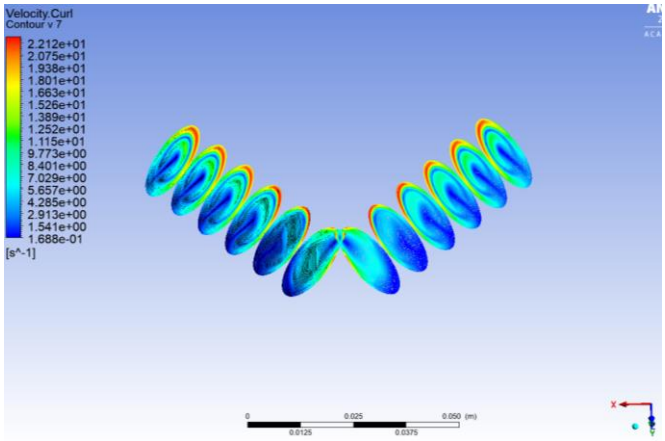

Figure 5.6: Vorticity Distribution at Various Pipe Cross-Sections in Y-Junction Flow, (A) with and (B) without Stenosis

5.1.3 Influence of Bifurcation Angle (BA) on Particle Trapping

In the previous sections, we have shown that the particle trapping exists in T-junction (BA= 90°) flow while no particle is trapped in Y-junction (BA=135°). We can therefore assume bifurcation angle may play an important role in particle trapping; how BA affects the particle trapping is investigated in this section. Six bifurcation models are built with BA ranging from 80° to 100°. Inlet Reynolds number is 360 and particle diameter is fixed at 1mm (5% of pipe diameter) which is the same as in the third case of section 3.2.2. The results show that particle trapping occurs only when the bifurcation angle is less than or equal to 90° as shown in Figure 5.7.

(A)

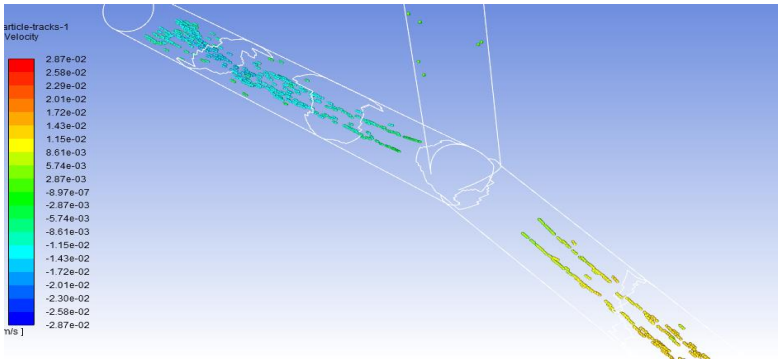
article-tracks-1
Velocity
2.87e-02
2.58e-02
2.29e-02
2.01e-02
1.72e-02
1.43e-02
1.15e-02
8.61e-03
5.74e-03
2.87e-03
-8.97e-07
-2.87e-03
-5.74e-03
-8.61e-03
-1.15e-02
-1.43e-02
-1.72e-02
-2.01e-02
-2.30e-02
-2.58e-02
-2.87e-02

(B)

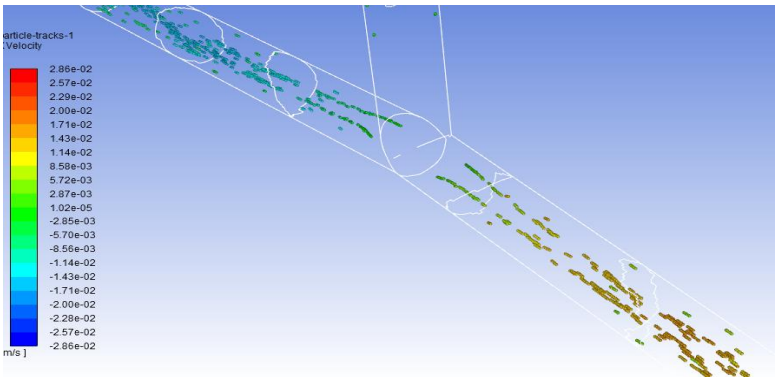
article-tracks-1
Velocity
2.86e-02
2.57e-02
2.29e-02
2.00e-02
1.71e-02
1.43e-02
1.14e-02
8.58e-03
5.72e-03
2.87e-03
1.02e-05
-2.85e-03
-5.70e-03
-8.56e-03
-1.14e-02
-1.43e-02
-1.71e-02
-2.00e-02
-2.28e-02
-2.57e-02
-2.86e-02

(C)

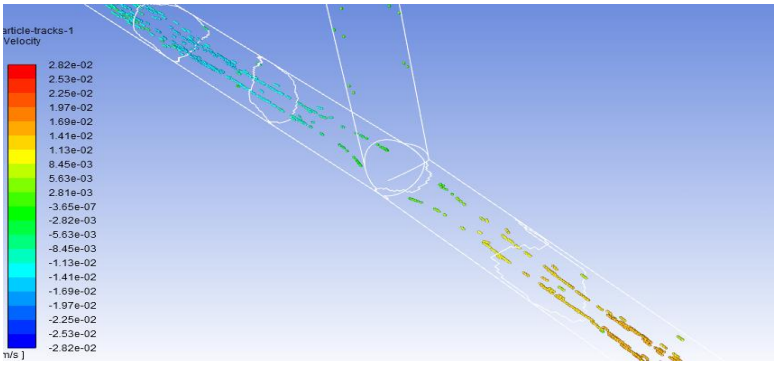
article-tracks-1
Velocity
2.82e-02
2.53e-02
2.25e-02
1.97e-02
1.69e-02
1.41e-02
1.13e-02
8.45e-03
5.63e-03
2.81e-03
-3.65e-07
-2.82e-03
-5.63e-03
-8.45e-03
-1.13e-02
-1.41e-02
-1.69e-02
-1.97e-02
-2.25e-02
-2.53e-02
-2.82e-02

(D)

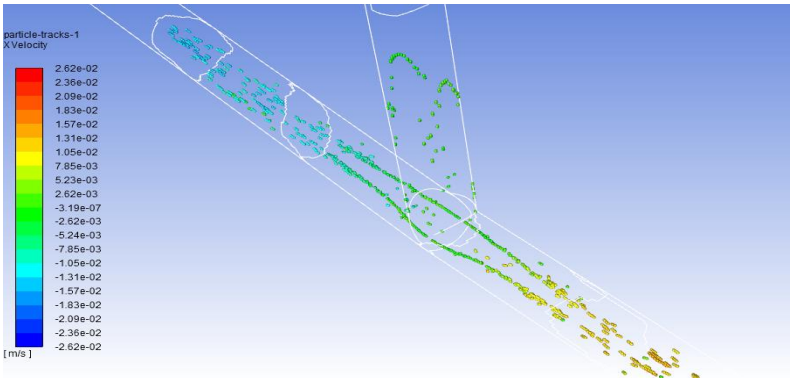
particle-tracks-1
X Velocity
2.62e-02
2.36e-02
2.09e-02
1.83e-02
1.57e-02
1.31e-02
1.05e-02
7.85e-03
5.23e-03
2.62e-03
-3.19e-07
-2.62e-03
-5.24e-03
-7.85e-03
-1.05e-02
-1.31e-02
-1.57e-02
-1.83e-02
-2.09e-02
-2.36e-02
-2.62e-02
[m/s]

(E)

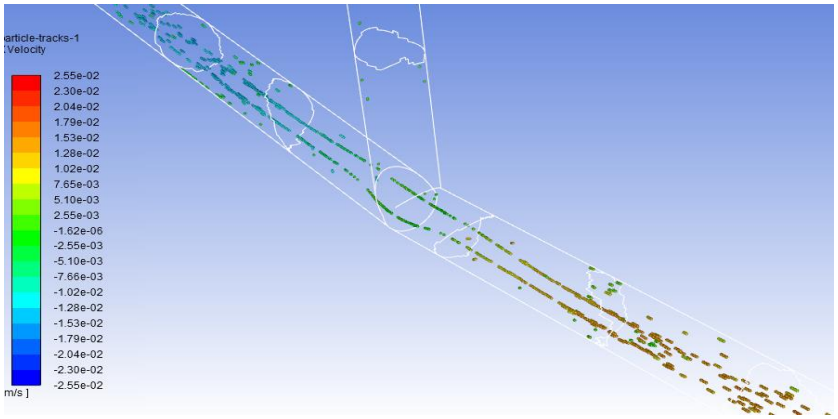

(F)

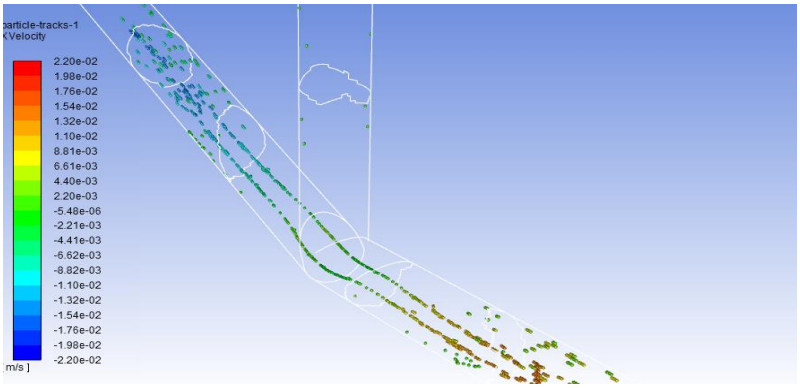

Figure 5.7: Particle Trapping in Different Models at BA= (A) 100°, (B) 95°, (C) 92.5°, (D) 87.5°, (E) 85° and (F) 80°

Table 5.1 shows the percentage of particle trapping for various bifurcation angles.

Bifurcation Angle (°)	Particle Trapping? (Y/N)	Trapped Number/Total Number	Trapped (%)
100	N	0/824	0
95	N	0/824	0
92.5	N	0/824	0
90	Y	507/1632	31.06%
87.5	Y	307/824	37.26%
85	Y	322/824	39.08%
80	Y	406/824	49.27%

Table 5.1: Percentage of Particles Trapped in Models with Different Bifurcation Angle

Table 1 shows that the particle trapping begins to occur when BA is between 90° and 92.5°. No particle trapping is found when BA is above 92.5°. This observation also explains why there was no particle trapped in Y-junction model (BA=135°). When BA changes near 90°, numbers of particles trapped changes dramatically. The percentage of particles trapped increases from 0% to 31.06% when BA is reduced from 92.5° to 90°. Particle trapping continues to increase as BA is further reduced to 80°.

5.2 Validation

In this section, we still study the geometry of Y-junction and create the model of Lu et al. [15-17] to validate the computation of laminar flow. All the pipes have the same diameter of 0.6 cm and the mother pipe is 1.8 cm long. After bifurcation, there are two daughter pipes at 90° angle. One daughter pipe is straight having a length of 4.8 cm. The other daughter pipe is straight for 0.9 cm after bifurcation before it undergoes 45° bending with a radius of 2.4 cm and then it becomes straight again for 2.4 cm until the end. The model of the bifurcation is shown in Figure 5.8.

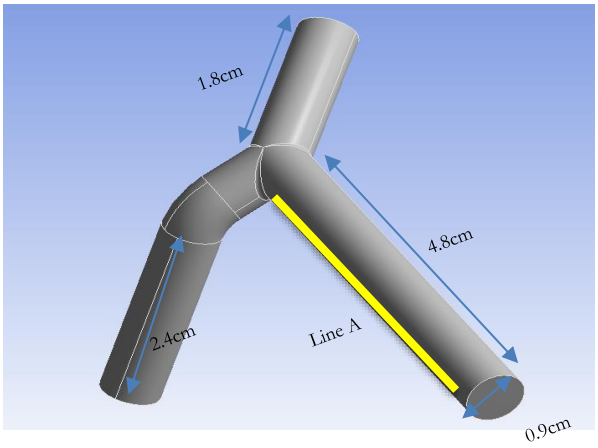

Figure 5.8: Geometry of Y-Junction for CFD Validation

Contours of pressure, velocity, wall shear stress and streamlines are shown in Figure 5.9. Wall shear stress (WSS) distribution at line A is shown in Figure 5.9 (A) which has good agreement with the results from Omid et al. [8] as shown in Figure 5.9 (B).

(A)

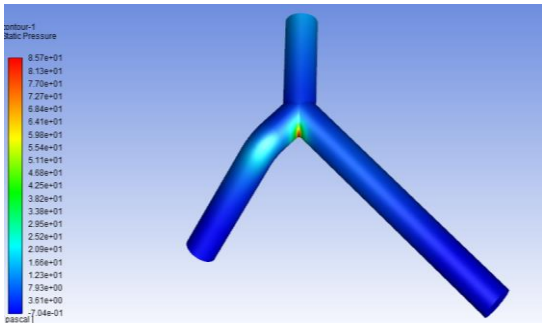

(B)

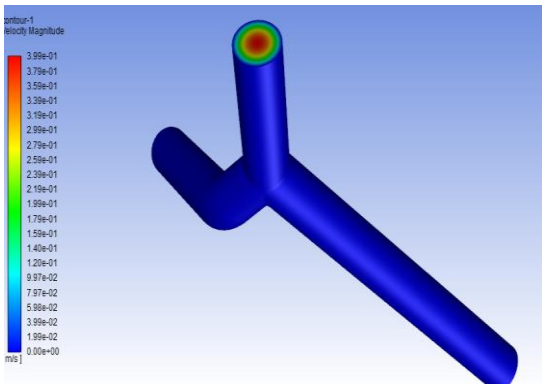

(C)

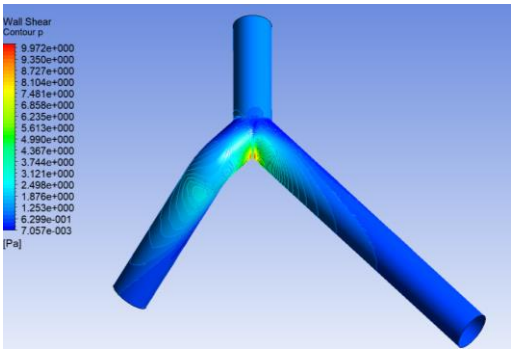

(D)

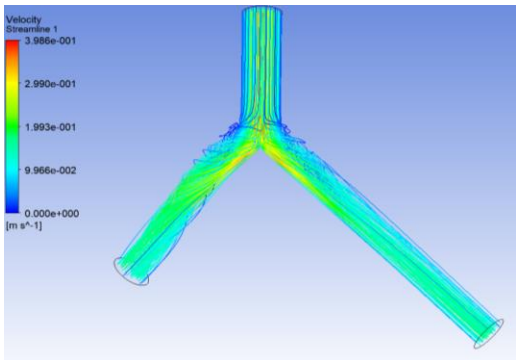

Figure 5.9: (A) Pressure Contours (B) Velocity Contours, (C) Wall Shear Stress Contours and (D) Streamlines for Lu's Y-Junction Model

(A)

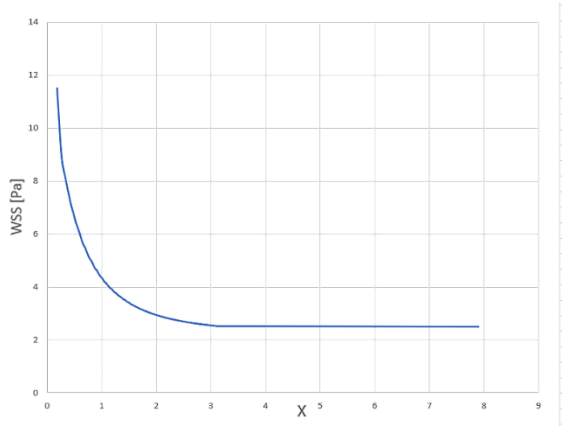

(B)

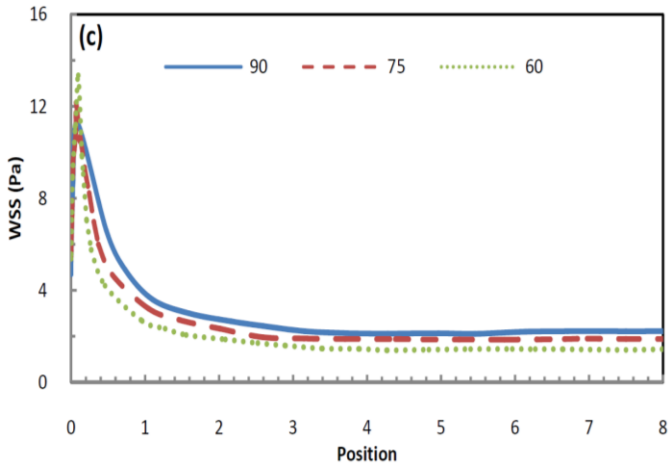

Figure 5.10: (A) WSS Distribution at Line A and (B) Simulation Results from Omid Arjmandi -Tash et al. [8]

Chapter 6 Conclusions

Eulerian simulations are performed by using the Discrete Phase Model (DPM) for two-phase flow with particles injected in different bifurcation models with bifurcation angle of an outlet pipe varying from 80° to 100° w.r.t the centerline of the inlet pipe (90° being the bifurcation angle of T-junction). By changing the average Reynolds number of the flow and the injected particles diameters, the mechanism of particle trapping is investigated in laminar flow. It is found that the particle trapping increases as the bifurcation angle decreases from 90° and becomes negligible as the bifurcation angle increases from 90°. This is a very important result which has never been reported in the previous literature. It is found that particle trapping in bifurcation flows is related to the particle diameters, Reynolds number and bifurcation angle in laminar flow. In addition, turbulent flow computations for T-junction flow are performed using the SST k-ω and Wray-Agarwal turbulence models. No particle trapping is observed in turbulent flow in T-junction flow. The influence of stenosis in Y-junction flow is also studied and analyzed. Stenosis has much bigger influence on vorticity than velocity in Y-junction flow. The results reported in this paper have implications in understanding the hemodynamic flows in arterial bifurcations without and with stenosis.

Chapter 7 Future Work

Several problems need to be addressed to extend the work in this thesis including further investigation on probability of particle trapping, more CFD validation, non-Newtonian fluid flow simulations as well as simulations in blood vessel models involving multiple branches of bifurcations and stenosis, and experimental work both in-vitro and in-vivo.

Current work in this thesis has investigated the influence of fluid Reynolds number, particle diameter and bifurcation angles on particle trapping; additional factors need to be considered in the future work. According to relevant literature, probability of particle trapping is also related to initial particles positions where they are injected; the trapping probability has almost a linear relationship with the depth of the initial position. At the same time, the exact bifurcation angle where particle trapping begins to appear may be addressed by optimizing the models.

More turbulent flow cases need to be considered in the future with emphasis on turbulence modeling especially for transient simulations. For the cases considered in thesis, it has been shown that both SST k-ω and WA turbulence models give very similar result; however other turbulence models should be considered and their influence on the accuracy of simulations should be investigated. The simulations with non-Newtonian model of blood flow should be performed and their influence on the accuracy of simulations should be investigated.

The simulations in other realistic vessel models should be considered for patient specific geometries. More detailed cardiovascular models can be created and optimized to study the particle trapping phenomenon. Blalock-Taussig (BT) Shunt, which is used in surgical procedure to address the problem of 'Blue Baby Syndrome" in new born children, can be a good application for the study of T-junction blood flow.

References

[1] Vigolo, D., Radl, S. and Stone, H. A., 2014, "Unexpected Trapping of Particles at a T Junction," Proc. Natl. Acad. Sci., U. S. A., Vol. 111, pp. 4770–4775.

[2] Meng H, et al., 2007, "Complex Hemodynamics at the Apex of an Arterial Bifurcation Induces Vascular Remodeling Resembling Cerebral Aneurysm Initiation," Stroke, Vol. 38, No. 6, pp. 1924–1931.

[3] Muth, C. M. and Shank, E. S., 2000, "Gas Embolism," New England J. of Medicine, Vol. 342, No. 7, pp. 476–482.

[4] Bass, R. M. and Longmore, D. B.,1969, "Cerebral Damage during Open Heart Surgery," Nature, Vol. 222, No. 5188, pp. 30–33

[5] Benjamin, T. B.,1962, "Theory of the Vortex Breakdown Phenomenon," J Fluid Mech., Vol. 14, pp. 593–629.

[6] Leibovich, S., 1978, "The Structure of Vortex Breakdown," Annual Rev. Fluid Mech., Vol. 10, pp.221–246.

[7] Shtern, V. and Hussain, F.,1999, "Collapse, Symmetry Breaking, and Hysteresis in Swirling Flows," Annual Rev. Fluid Mech., Vol. 31, pp. 537–566.

[8] Arjmandi-Tash, O., Razavi, S. E. and Zanbouri, R., 2011, "Possibility of Atherosclerosis in an Arterial Bifurcation Model," Bio Impacts, Vol. 1, No. 4, pp. 225-228.

[9] Antonova, N., Xu, D., and Kaliviotis, E., 2015, "Stenosis Effects on the Fluid Mechanics of the Common Carotid Artery Bifurcation for Unsteady Flows," Journal of Mechanics in Medicine and Biology, Vol. 15, No. 2, p. 1540008.

[10] Menter, F. R., "Two-Equation Eddy-Viscosity Turbulence Models for Engineering Applications," AIAA Journal, Vol. 32, No. 8, August 1994, pp. 1598-1605.

[11] Han, X., Rahman, M. M., and Agarwal, R. K., 2018, "Development and Application of a Wall Distance Free Wray-Agarwal Turbulence Model," AIAA Paper 2018-0593, AIAA SciTech Forum, Kissimmee, FL, 8-12 January 2018.

[12] ANSYS Inc., ANSYS 12.0 User Manual, 2012.

[13] Kurose, R. and Komori, S., 1999, "Drag and Lift Forces on a Rotating Sphere in a Linear Shear Flow," J. Fluid Mech., Vol. 384, pp.183–206.

[14] Mclaughlin, J.B., 1991, "Inertial Migration of a Small Sphere in Linear Shear Flows," J. Fluid Mech., Vol. 224, pp.261–274.

[15] Lu, X. Y., Zhang, L., and Wang, W., 2002, "Breaking Symmetry in Non-Planar Bifurcation: Distribution of Flow and Wall Shear Stress," Bio-rheology, Vol. 39, No. 3-4, pp. 431-436.

[16] Chen, J. and Lu, X. Y., 2004, "Numerical Investigation of the Non-Newtonian Blood Flow in a Bifurcation Model with a Non-Planar Branch," Journal of Biomechanics, Vol. 37, No. 12, pp. 1899-1911.

[17] Chen, J. and Lu, X. Y, 2006, "Numerical Investigation of the Non-Newtonian Pulsatile Blood Flow in a Bifurcation Model with a Non-Planar Branch," Journal of Biomechanics, Vol. 39, No. 5, pp. 818-832.

Vita

Qihang Xu

Degrees: M.S. Mechanical Engineering, Washington University in St. Louis, May 2020
B.E. Mechanical Engineering, Tianjin University, July 2018

Publications: Q. Xu and R. K. Agarwal, "Blood Flow Simulations of Particle Trapping in Models of Arterial Bifurcations," ASME Fluids Engineering Division Summer Meeting (FEDSM), Orlando, FL, 12-16 July 2020.

May 2020

Blood Flow Simulations of Particle Trapping in Models of Arterial Bifurcations, Qihang Xu, M.S. 2020